جمهورية العراق
وزارة التعليم العالي والبحث العلمي
جامعة بابل
كلية العلوم للبنات
قسم فيزياء الليزر

الوصلات الجزيئية القائمة على الروتاكسان للتطبيقات الالكترونية والالكترونات البصرية

رسالة مقدمة

الى مجلس كلية العلوم في جامعة بابل

وهي جزء من متطلبات نيل درجة الماجستير في علوم فيزياء الليزر وتطبيقاته

من قبل الطالبة

هبه عباس محمد

بإشراف

أ.م.د عدي اركان عباس الجبوري

أ.م.د. حسين نعمه نجيب الخيكاني

1445 A.H

2023 A.D

Republic of Iraq

Ministry of Higher Education and Scientific Research

University of Babylon

College of Sciences for Women

Department of Laser Physics

Rotaxane Based Molecular Junctions for Electronic and Optoelectronic Applications

A Thesis

Submitted to the Council of the College of Sciences for Women / University of Babylon in Partial Fulfillment of The Requirements for the Degree of Master of Science in Laser Physics and its Applications.

By

Hiba Abbas Mohammed

Supervised by

Assist. Prof.

Dr. Oday A. Al-Owaedi

College of Science for women

University of Babylon

Assist. Prof.

Dr. Hussein Neama Najeeb

College of Science for women

University of Babylon

2023 A.D **1445 A.H**

بِسْمِ اللَّهِ الرَّحْمَٰنِ الرَّحِيمِ

يَرْفَعِ اللَّهُ الَّذِينَ آمَنُوا مِنْكُمْ وَالَّذِينَ أُوتُوا الْعِلْمَ

دَرَجَاتٍ وَاللَّهُ بِمَا تَعْمَلُونَ خَبِيرٌ ۝

صَدَقَ اللهُ العَظِيم

سورة المجادلة الآية (١١)

Dedication

To the one who led the hearts and minds of mankind to a safe harbor, the first teacher of humanity, ***Muhammad, may God bless him and grant him peace.***

To the one with tender breasts, the one with the umbilical cord whose trace still remains in me until now.. ***my mother.***

*To the one who illuminated my path, the source of tenderness...****my father***

To the life partner and the firm trunk that we lean on and enslaved to his shadow. You are the spark for me when my light blew out… ***my supportive lover husband***

*To the source of love, tenderness and loyalty, who supported me with her prayers****… my mother-in-law****.*

To the address of brotherhood and the ember of sincerity .. ***my brothers****.*

To those who were planted in hope, so that I can move forward whenever despair appears in my soul... ***my sisters****.*

*To the pleasures of my liver, the seeds of the future and the labors of my knowledge...****my offspring, Ali, Mayar, Ridha, may God protect them****.*

To the support and forearm, in the orbit of your friendship revolves my happiness.. ***my friends.***

Hiba (2023)

Acknowledgements

First of all, I would like to thank the supreme power "Allah" the one has always guided me to work on the right path of life the most merciful who helped me in achieving this goal

I would like to express my remarkable thanks of gratitude to my supervisor ***Assistant Prof. Dr. Oday A. Al-Owaedi*** *who gave me the golden opportunity to make this work possible . His guidance and advice carried me through all the stages of writing my project and the Headmaster of Laser Physics Department, the staff and the dean of the College of Science for Women for their assistance.*

I would like to express fully gratefulness to my supervisors ***Assistant Prof. Dr. Hussein Neama Najeeb*** *for his guidance and support throughout my study.*

Hiba

Examination Committee Certification

We certify that after reading this thesis, entitled: **"Rotaxane Based Molecular Junctions for Electronic and Optoelectronic Applications "**, and as committee, examined the student **"Hiba Abbas Mohammed"** its contents and that in our opinion it meets the standards of a thesis for the Degree of Master of Science in Laser Physics and its Application.

Signature:
Name: **Dr. Ahmed Kamal Ahmed**
Title: Professor
Date: / / 2023
(Chairman)

Signature:
Name: **Dr. Ghaleb Ali Al-Dahash**
Title: Professor
Date: / / 2023
(Member)

Signature:
Name: **Dr. Oday A. Al-Owaedi**
Title: Assistant Professor
Date: / /2023
(Member)

Signature:
Name: **Dr. Nizar Salem Shanan**
Title: Assistant Professor
Date: / / 2023
(Member)

Signature:
Name: **Dr. Hussein Neama Najeeb**
Title: Assistant Professor
Date: / / 2023
(Member)

Approved by the Dean of College
Signature:
Name: **Dr. Abeer Fawzi Al-Rubaie**
Title: Professor
Address: Dean of the College of Science for Women.
Date: / / 2023

Supervisor certificate

We certify that this thesis entitled **"Rotaxane Based Molecular Junctions for Electronic and Optoelectronic Applications"** was prepared by the student **(Hiba Abbas Mohammed)** under our supervision at the department of Laser physics, College of Science for Women, University of Babylon, as a partial fulfillment of the requirements of the degree of Master of Science in laser physics and its applications.

Signature:

Name: ***Dr.Oday A. Al-Owae***

Title: **Assistant. Prof.**
(Supervisor)
Date: / / 2023

Signature:

Name: ***Dr.Hussein Neama Najeeb***

Title: Assistant. Prof.
(Supervisor)
Date: / / 2023

Head of the Department Certificate

In view of the available recommendations, I forward this dissertation for debate by the examining committee.

Signature:
Name: ***Dr.Jinan Ali Abd***
Title: **Professor**
(Head of Laser Physics Department)
Date: / /2023

List of Abbreviations

Abbreviation	Physical meaning
B.E.	Binding energy
BSSEC	Basis set superposition error correction
BJ	Break Junction
CA	Ceperly and Alder
CP	Counterpoise correction
DFT	Density Functional Theory
DNA	Deoxyribonucleic Acid
EXC	Exchange Correlation energy
FOM	Figure of Merit
GF	Green‘s function
GGA	Generalized gradient approximation
HOMO	High occupied molecular orbitals
KS	Kohn and Sham
LAOBs	Localised Atomic Orbital Basis Sets
LCAO	Linear Combinations of Atomic Orbitals
LCAOBs	Linear Combinations of Atomic Orbitals Basis set
LDA	Local density approximation
LUMO	Lowest unoccupied molecular orbitals
MIMs	Mechanically Interlocked Molecules
MORF	Metal-Organic Rotaxane Frameworks
NEGF	Non-Equilibrium Green's Function
NDR	Negative Differential Resistance
NTPs	Nucleoside Triphosphates
PBE	Perdew, Burke and Ernzherhof
PH	Potential of hydrogen ions

List of Abbreviation

PZ	Perdew and Zunger
QTT	Quantum Transport Theory
R-G	Runge-Gross theorem
SALI	Surface-Induced Absorption Layer Inference
SCF	Self-Consistent Field
SIESTA	Spanish Initiative for Electronic Simulations with Thousands of Atoms
STM	Scanning Tunnelling Microscopy

List of Figures

Figure No.	Figure Caption	Page No.
1.1.	Graphical representation of Rotaxane	**3**
1.2.	Applications of the Rotaxane molecule system	**4**
2.1.	A Schematic Illustration of the Self-consistent DFT Cycle.	**24**
2.2.	Illustrating the Counterpoise method to calculate the binding energy. (a) Represents the basis functions for total system where atoms are white colour and the basis functions of the atoms are gray. (b) and (c) show the basis function for the individual monomers whereas (d) and (e) represent the counterpoise correction, every single molecule is evaluated with the same basis function as the total system in (a).	**33**
2.3.	Theoretical One-dimensional Transport Model	**37**
3.1.	The optimized geometries at ground state of all molecules. The red balls are oxygen atoms, grey are carbon atoms, the white ones are hydrogen atoms, and the blue ones are nitrogen atoms.	**45**
3.2.	The optimized geometry at ground state of macrocycle wheel. The red balls are oxygen atoms, grey are carbon atoms, the white ones are hydrogen atoms, and the blue ones are nitrogen atoms.	**46**

List of Figures

3.3.	The optimized geometries at ground state of all molecular junctions.	**48**
3.4.	Represents the transmission coefficient T(E) as a function of electrons energy of all molecular junctions.	**51**
3.5.	Represents the transmission coefficient T(E) as a function of the number of electrons transferred from molecule to electrodes of all molecular junctions.	**52**
3.6.	Represents the electrical decay constant (β) as a function of Fermi energy of all molecular junctions.	**54**
3.7.	Represents the binding energy (B.E.) between molecule and gold electrodes of all molecular junctions.	**56**
3.8.	Represents the electrical conductance (G/G_0) as a function of Fermi energy of all molecular junctions.	**58**
3.9.	Represents the current-voltage (I-V) characteristics of all molecular junctions.	**60**
3.10.	Represents the thermopower (S) as a function of Fermi energy of all molecular junctions.	**62**
3.11.	Represents the electronic figure of merit (ZT_e) as a function of Fermi energy of all molecular junctions.	**64**
3.12.	Represents the power factor (ZT_e) versus the number of wheels of all molecular junctions.	**65**

Table of Contents

Table of Contents		
NO.	Subject	Page NO.
	Supervision Certification	I
	Dedication	II
	Acknowledgments	III
	Abstract	IV
	Table of Contents	VI
	List of Abbreviations	IX
	List of Symbols	XI
	List of Figures	XV
	List of Tables	XVI
Chapter 1 : Introduction		
NO.	Subject	Page NO.
1.1.	Introduction	1
1.2.	Rotaxane Molecules	2
1.3.	Molecular Nano Technology	4
1.4.	Literature review	6
1.5.	The Aims of the Study	12
Chapter 2 : Density Functional Theory		
NO.	Subject	Page NO.
2.1.	Introduction	13
2.2.	Schrödinger Equation and Variational Principle	14
2.3.	The Hohenberg-Kohn Theorems	18

2.4.	Kohn-Sham Method and Self-Consistent Field	21
2.5.	The Exchange-Correlation Potential	25
2.5.1.	Local Density Approximation (LDA)	26
2.5.2.	Generalized Gradient Approximation (GGA)	27
2.6.	SIESTA	29
2.6.1.	Localised Atomic Orbital Basis Sets (LAOBs)	30
2.6.2.	Basis Set Superposition Error Correction (BSSE)	32
2.6.3.	Structure Optimisation	34
2.7.	Green's Function Scattering Formalism	34
2.8.	Landauer Formula	35
2.9.	GOLLUM Code	39
2.10.	Electric and Thermoelectric Properties	40
Chapter 3 : Results and Discussions		
NO.	**Subject**	**Page NO.**
3.1.	Structural and Morphological	44
3.2.	Electronic Properties	50
3.2.1.	Transmission Coefficient T(E)	51
3.2.2.	The Charges Transfer (Γ)	52
3.2.3.	Electrical Decay Constant (β)	54
3.2.4.	Binding Energy (B.E.)	56
3.3.	Electric and Thermoelectric Characteristics	58
3.3.1.	Electrical Conductance (G/G_0)	58
3.3.2.	Current-Voltage Characteristics	60
3.3.3.	Thermopower (S)	62
3.3.4.	Electronic Figure of Merit (ZT_e)	63
3.3.5.	Power Factor(P)	65

Chapter 4 : Conclusions and Future Works		
NO.	**Subject**	**Page NO.**
4.1.	**Conclusions**	**67**
4.2.	**Future Works**	**68**

Abstract

The field of nanotechnology aims of making electronic components, eventually achieving sub-2 nm length scales. This work aims to study and understand of such components by a theoretical investigation of structural, electronic, electrical and thermoelectric properties of molecular nano-junctions consist of single molecule connected to two gold reservoirs **Au | Molecule | Au**. All characteristics of molecular systems under investigation in this thesis have been probed using the density functional theory (DFT) methods and using a combination of DFT methods and Quantum Transport Theory (QTT). Rotaxane molecule is classified as a kind of mechanically interlocked molecule composed of a linear molecule called an axle and an organic ring. This study investigate the properties of Rotaxane molecular junctions with different numbers of rings ranging from one to five rings. In addition to the morphological and structural aspects, the number of atoms increased from 149 atom for molecule R-1 to 422 atom for molecule R-5. The DFT calculations predicted an obvious impact of the number of organic rings on all properties, since the HOMO-LUMO gap shrunken from -1.14 eV for molecule R-1 to -1.05 eV for molecule R-5. Whereas, the transmission coefficient increased from 1.6×10^{-4} for R-1 to 2.3×10^{-3} for R-5. The structural variation by increasing the rings of course increased the atoms as mentioned, and that increased the transferred electrons from molecule to electrodes (Γ) dramatically, since the value of Γ for molecule R-1 is 196.6 electron, while it is 542 electron for R-5. The binding energy (B.E.) values fluctuated from -0.46 eV for molecular junction R-1, and it lowered to -0.25 eV for R-2, then it is raised to -0.61 eV for R-3, and again it decreased to -0.32 eV for R-4, and finally it increased to -0.72 eV for R-5. The effect of number of organic rings remains an important factor even in presence of temperature (T), since the values of electrical conductance (G/G0) as a function of Fermi energy were 1.5×10^{-4} for molecule R-1, while it

is 2.2×10^{-3} for R-5. In contrary, the values of the threshold voltage (V_{th}) were 0.47 eV for R-1 and it is 0.42 eV for R-5. Furthermore, the sign of Seebeck coefficient (S) was negative and its values were -29 μVK^{-1} for R-1 and it is -19 μVK^{-1} for R-5. The computed values of electronic Figure of Merit (ZT_e) were 0.05 for R-1, and 0.006 for R-5.

الخلاصة

يهدف مجال تكنولوجيا النانو إلى جعل المكونات الإلكترونية ، مما يؤدي في النهاية إلى تحقيق مقاييس طول أقل من 2 نانومتر. هذا العمل يهدف إلى دراسة وفهم هذه المكونات من خلال التقصي النظري في الخواص الهيكلية والإلكترونية والكهربائية والكهروحرارية للوصلات النانوية الجزيئية التي تتكون من جزيء واحد مرتبط بخزانين من الذهب Au | Molecule | Au. تم فحص جميع خصائص الأنظمة الجزيئية قيد الدراسة باستخدام طرق نظرية الكثافة الوظيفية (DFT) وطرق نظرية الكثافة الوظيفية المعتمدة على الزمن (TD-DFT). يصنف جزيء الروتاكسين على أنه نوع من الجزيئات المتشابكة ميكانيكيا المتكونة من جزيء خطي يسمى المحور والحلقة العضوية. يدرس هذه العمل خصائص وصلات الروتاكسين الجزيئية بأعداد مختلفة من الحلقات تتراوح من (5 – 1). بالإضافة إلى الجوانب المورفولوجيا والهيكلية, حيث ازداد عدد الذرات من 149 ذرة للجزيئة R-1 إلى 422 ذرة للجزيئة R-5.توصلت حسابات DFT الى وجود تأثير واضح لعدد الحلقات العضوية على جميع الخصائص، حيث تقلصت فجوة (HOMO-LUMO) من 1.14 eV- لجزيئة R-1 إلى 1.05 eV - للجزيئة R-5في حين ارتفع معامل الانتقال من 1.6×10^{-4} للجزيئة R-1 إلى 2.3×10^{-3}للجزيئة R-5. التباين الهيكلي عن طريق زيادة الحلقات أدى بالطبع الى زيادة الذرات كما ذكرنا, وبالنتيجة ازدادت الإلكترونات المنقولة من الجزيئة إلى الأقطاب الكهربائية (Γ) بشكل كبير, حيث أن قيمة Γ للجزيئة R-1 هي 196. 6إلكترون ، بينما كانت 542 إلكترون للجزيئة R-5 . تذبذبت قيم طاقة الربط (B. E) من - 0.46 eVللجزيئة, R-1، وانخفضت إلى 0.25 eV - للجزيئة, R-2، ثم تم رفعها إلى 0.61 eV- للجزيئة R-1، ومرة أخرى انخفضت إلى 0. 32 eV- للجزيئة R-4، وأخيرا زادت إلى 0. 72 eV- للجزيئة R-5 . ان تأثير عدد الحلقات العضوية عاملا مهما حتى في وجود درجة الحرارة (T)، حيث كانت قيم التوصيل الكهربائي (G/G_0) كدالة لدرجة الحرارة T هي 1.5×10^{-4} للجزيئة R-1 ، بينما كانت 2.2×10^{-3} للجزيئة R-5 . بالمقابل ، كانت قيم جهد العتبة (V_{th}) 0.47 eV للجزيئة R-1 و 0.

42 eV للجزيئة R-5 .علاوة على ذلك ، كانت علامة معامل سيباك (S) سالبة وقيمتها $-29\ \mu VK^{-1}$ للجزيئة R-1 و $-19\ \mu VK^{-1}$ للجزيئة R-5. كما كانت القيم المحسوبة لرقم الجدارة الالكتروني 0.05 (ZT_e)للجزيئة R-1، و 0.006 للجزيئة R-5.

1.1. Introduction

The field of molecular electronics is based on exploiting molecules as fundamental units for computing and other electronic functions. This gives molecular electronics an attractive role in the technology field because it provides the ultimate size for system scaling. There have been numerous past efforts to develop this field which are focused on characterization, fabrication, and design of such devices. Today electronic devices reduced to sizes on the molecular scale are considered a major step to advances in modern technology. The need for molecular electronics originates from the increase in demand for more powerful computational devices and this demand translated for realistic systems with silicon –based chips was demonstrated by Gordon Moore in 1965 [1] which is known as Moore's Law that states every 18-24 months the number of transistors per chip will double. This cannot continue indefinitely because of an acceptable charge leakage that occurs when the thickness of oxide layers within silicon chip approaches a few atoms [2]. To go beyond the sub-10 nm scale, industry must find alternative approaches and materials and, it is hoped that molecular electronics will play a key role in this. Molecular electronics provides a new concept of synthesis and design for continued reduction in the size of electronics components, by starting with molecular building blocks. The original idea for molecular electronics appeared in 1974 when Aviram and Ratner suggested using molecules as an alternative to silicon chips [3]. Their suggested theoretical rectifier was a starting point for development in this field, which leads to a multidisciplinary approach combining the efforts of researchers from different fields, such as chemists, engineers, experimental and theoretical physicists. It is through a combination of theory and experiment that progress in understanding the electronic behaviour of molecules is made. In addition, the progress in

computing power and modelling tools enables realistic systems to be simulated and achieve results approximately close to experimental measurements. On the other hand, significant progress in experimental techniques, such as scanning tunnelling microscopy STM [4], gives the ability to study the electronic single molecule properties through imaging, combined with measurement of the electronic response of the molecules. The main challenge in this field is to find convenient molecular functions, materials and techniques to reach desirable properties for electronic devices. Rotaxane molecule is one possible candidate for molecular electronics, due to its unique properties which are particularly varied due to the unique characteristics of these molecules.

This thesis invistage the morphological, structural, electrical and thermoelectric properties of Rotaxane molecular junctions using density functional theory methods (DFT) and Quantum Transport Theory (QTT).

1.2. Rotaxane Molecules

One of the best candidates for molecular machines are mechanically interlocked molecules, such as rotaxanes, because (i) the mechanical bond permits a wide range of mutual arrangements of the molecular components while conferring stability on the system; (ii) the interlocked architecture restricts the amplitude of the motion of the intercomponent in three dimensions; and (iii) the stability of a particular arrangement is determined by the strength of the intercomponent in the arrangement. These systems initially attracted attention due to their intriguing topology and associated synthetic challenge, but recent research has shown that they are also attractive as nanoscale switches for molecular electronics and nanoelectromechanical systems due to their electrical properties and bi- or multistable behavior[5]. Molecular machines and motors are based on the

interlocked chemical compounds known as rotaxanes. These compounds' names are derived from the Latin terms rota, which means wheel or axle, and axis, which means chain. Rotaxanes consist of (at least) two interlocked macrocycles or "rings," which are essentially an axle-like molecule surrounded by a macrocyclic compound and ended by bulky groups (stopper) that prohibit disassembly . Because it is simple to visualize the motions of their molecular components, rotaxanes are appealing systems for the building of molecular machines as shown in Figure 1.1.[5]

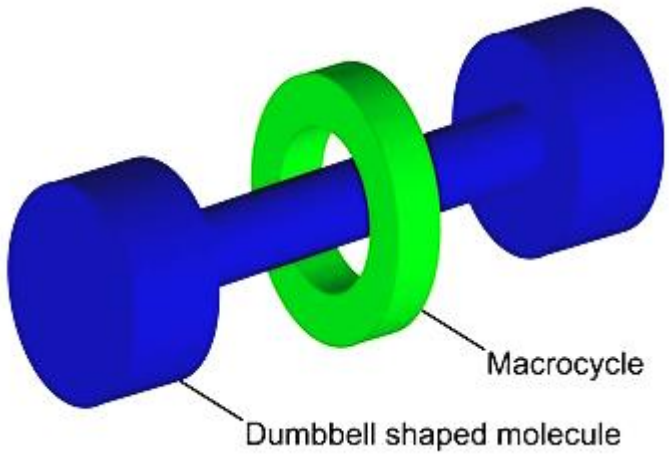

Figure 1.1. Graphical Representation of a Rotaxane[5].

Rotaxane dendrimers are dendritic molecules with mechanical bonds that resemble rotaxane to connect their constituent parts. Their synthesis, characteristics, and potential applications are explained depending on where rotaxane-like features are introduced. Rotaxane dendrimers are divided into three types: Type I, II, and III rotaxane dendrimers, which integrate rotaxane-like features at the core, termini, and branches, respectively. Several distinct types of macrocycles are employed as the ring component in the templated synthesis of rotaxane dendrimers. Several factors should be carefully examined in the synthesis of rotaxane dendrimers, including the binding affinity of the macrocycle (ring) and axle

(rod). The characteristics of these rotaxane dendrimers are very distinct from those of the individual rotaxanes or dendrimers, and frequently a mix of both. Rotaxane dendrimers might be used in molecular nanoreactors, drug transport, and gene delivery, as shown in Figure 1.2 [6].

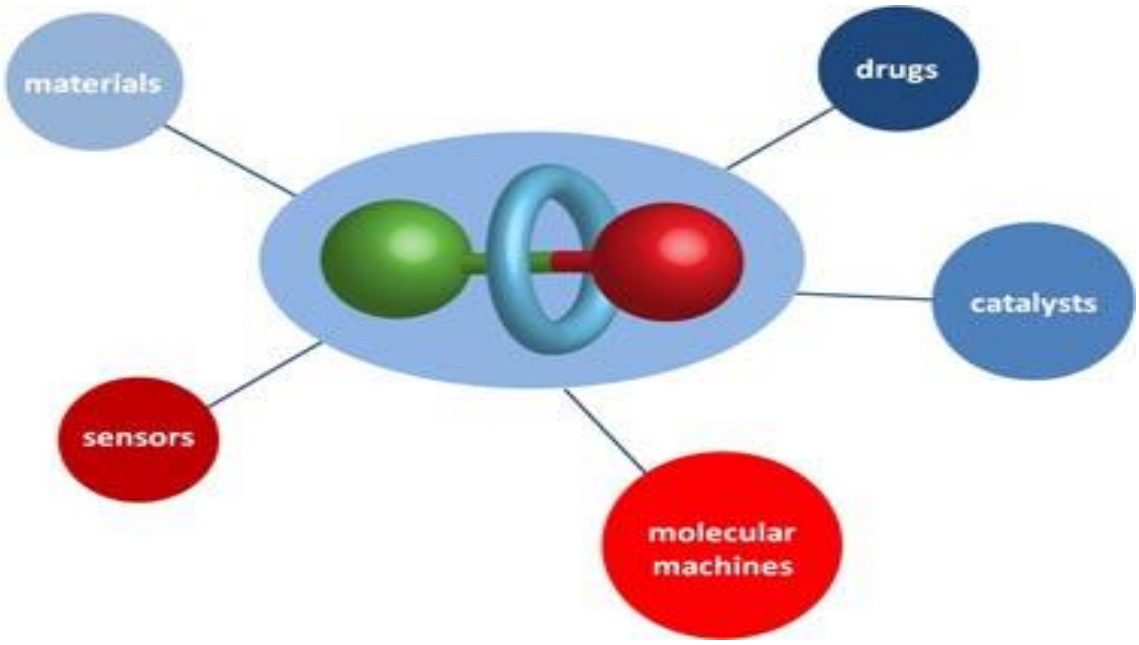

Figure 1.2. Applications of the Rotaxane Molecule System[6].

1.3. Molecular Nano Technology

One of the final objectives of nanotechnology is to construct electronic devices out of single molecules. Electron transport through molecules connected to electrodes must be measured, managed, and understood in order to accomplish this. Because of its potent monitoring and control capabilities, the combination of single-molecule junctions with various multimodal control systems has recently been widely used to investigate important physical and chemical phenomena[7]. The concept of employing single molecules as active electronic components served as the inspiration for the creation of a variety of experimental systems to

investigate their electronic transport characteristics. One of these has the shape of a single molecule sandwiched between two metal electrodes, known as a single-molecule junction.

Utilizing the break junction technique is the most popular way to create complimentary junctions. Mechanical fractured junctions and electrochemical break junctions are the two types of single-molecular junctions that are most frequently encountered [8, 9]. Our basic grasp of the concepts needed to actualize molecular-scale electronic components, from resistive wires to reversible switches, has greatly benefited from the study of single-molecule junctions in a metal-molecule-metal motif. New methods to study metal-molecule-metal junctions with multiple probes are being developed as a result of the success of these techniques and uncreased interest of other fields in single-molecule level characterization. New studies which go beyond electronic transport characterization, focus on the basic and practical aspects of mechanical, optical, and thermoelectric properties at the atomic and molecular level[9].

Since many nanoelectronic devices have layered structures and the behavior of the electron at the interface influences the electronic properties of the final component and because multiple junctions and the interface have different electron transfer mechanisms than bulk materials, studying the electronic structure of the interface used in nanoelectronics is one of the key methods for comprehending the nature of electron transfer in this field. Depending on the purpose and the nature of the charge transfer, the molecular units used to make molecular junctions can be either organic or inorganic compounds make up the majority of these junctions [9,10].

One of the most important applications of nanoscience and nanotechnologies is the medical applications. In this context, the Rotaxane nano junctions play an important role. Nanomedicine is a notion that came into existence with the new millennium and is anticipated to offer solutions

to some of the unresolved issues in contemporary medicine [11]. Nanomedicine provides fresh possibilities in a number of pressing fields, including the treatment of cancer, viral and bacterial infections, medical imaging, tissue regeneration, and theranostics. The recent focus on the nanomedicine applications of nanomaterials having interlocked structures, interlocked systems, specifically rotaxanes have been incorporated into some of these chemical platforms in an effort to improve their performance. Recently, a significant progress has been made in the production and use of mechanically interlocked molecules (MIMs) [12]. MIMs are starting to transition from being fundamental research subjects, examined for their synthetic chemistry and molecular complexity, to functional systems with possible real-world applications [13]. They have been employed in the creation of molecular machines[14], chemosensors[15], catalysis[16]. The use of them for biomedical purposes is another fascinating area of study, which needs more studies and invistagations, and the rotaxane molecule is one of the best candiates for these applications [16].

1.4. Literature Review

Noelia Fontes *et al*, in 2011 [17] are conducted a study on the use of molecular switches based on organic compounds in the field of molecular electronics. They analyzed the characteristics and expected performance of these molecular switches in various electronic applications. The study elucidated how to design and assemble these switches and how they can be used to achieve specific functions such as switching and controlling current flow. The study provides valuable insights into the use of organic compounds as a means of molecular-level control in electronics.

In 2012, V. Nicholas Vukotic and Stephen J. Loeb[18], have studied the design and synthesis of unconventional coordination polymers. They utilized rotaxanes as primary linkers in these compounds. The main idea behind this study is to create coordination polymers that incorporate rotaxanes as part of their structure. A rotaxane is a type of molecule containing a movable ring that slides along a specific axis within another molecule. It can be visualized as a ring sliding inside a tube. These rotaxanes were used as linkers to connect polymer units together. This allows for the creation of complex polymer structures composed of coordination units and rotaxanes. These polymer structures may exhibit unique and intriguing properties due to interactions between the constituent molecules as linkers. This opens up new avenues for investigating the properties and potential applications of such materials.

In 2013, Clavel Caroline and colleagues [19] are conducted a study exploring new and exciting applications of rotaxanes in the field of molecular chemistry. This study stood out due to the design of a "molecular key for rotaxanes," which is a unique type of molecular tether. It's worth noting that rotaxanes are molecules that consist of a movable ring sliding along an axis within another molecule .The molecular key for rotaxanes in this study relies on the molecule's response to changes in the surrounding acidity (pH). When the pH changes, the molecule can transition between different states, acting like a "key" that can open or close the rotaxane. This type of control over molecular structures opens doors to multiple applications in fields such as molecular transport, environmental sensing, and pharmaceuticals .This study is innovative because of its clever design based on acidic-alkaline interactions. It contributes to the development of new tools and systems that rely on rotaxanes and leverage changes in pH in the surrounding environment to control molecular structures effectively.

In 2014, Bruns Carson J. and J. Fraser Stoddart [20], are focused on the concept of "molecular muscles based on rotaxanes" and their promising applications. Rotaxanes are a type of molecules that include a movable ring sliding within another molecule and function similarly to biological muscles in living organisms. In this study, a system based on rotaxanes was designed, which could be controlled by changes in pH in the surrounding environment. When the pH changes, this system can control the movement of rotaxanes in a manner similar to the movement of muscles.This study represents an exciting starting point for new applications in fields such as molecular actuation, molecular transport, and the development of interactive systems that rely on rotaxanes as vital components. Furthermore, it contributes to a better understanding of acidic-alkaline reactions in complex molecular systems.

In 2015, Hong Li and Da-Hui Qu [21] are summarized recent advancements in the field of new-type molecular switches. This study addressed various developments and innovations in the design and application of molecular switches that respond to a range of stimuli.The aim of this type of research is to develop molecular switches that interact with specific factors such as changes in temperature, light, acidity, and more. This opens doors to multiple applications in areas like molecular transportation, sensing, and molecular electronics.The summary of this research helps in understanding the latest techniques and applications in the field of molecular switches and the progress achieved in this field.

Noël Pairault and colleagues in 2016 [22], have focused on designing molecular structures based on rotaxanes that could be used in applications related to the life sciences. Rotaxanes are molecules that include a movable ring sliding along an axis within another molecule. In this study, these

rotaxanes were utilized to construct tailored architectural structures capable of performing specific functions in the field of life sciences. Applications such as precise drug delivery to specific locations in the body or the design of drug delivery systems rely on the innovative architectural structures described in this study. These research findings offer new possibilities for medical and biological applications, contributing to the development of more accurate and effective technologies in this field.

Milan David C., *et al*, in 2017[23], have published an important study that focused on the detailed analysis of electrical conduction through a supramolecular assembly containing rotaxane and hexayne. Rotaxane is a type of molecule that includes a movable ring that slides along an axis within another molecule, while hexayne is a molecule composed of six carbon units .The results showed that the arrangement of these molecules could significantly impact electrical conduction at the nanoscale. This discovery can serve as the foundation for designing and developing extremely small electronic systems that rely on molecules and effectively utilize nanoscale electrical conduction .In general, this study contributes to our better understanding of molecular-level electrical conduction and opens up new possibilities for potential applications in the fields of nanotechnology and molecular electronics.

In 2018, Mathew Paven Thomas, and Fengzhou Fang [24], have provided an overview of advancements in the field of molecular electronics. They highlighted recent developments in designing and using molecules as electronic devices at the molecular level. Topics such as molecular applications in nanowires, molecular switches, electrical conduction through molecules, and molecular information storage were discussed. This study underscores the significance of research in the field

of molecular electronics and how it can lead to innovative technologies in electronics and information storage. In summary, this study reflects recent progress in the field of molecular electronics and offers a brief insight into potential applications and future challenges in this field.

In 2019 [25], Schröder Hendrik V.*et al*, have shed light on recent advancements in electrochemically switchable rotaxanes. Rotaxanes are molecules that consist of a movable ring that slides along an axle within another molecule. The study reviewed new applications and innovations in this field, particularly focusing on the ability to control these rotaxanes through electrochemical chemistry. The study discussed modern methods and techniques that enable this control and how it can have positive effects in areas such as molecular transport and sensing applications. Overall, this study represents progress in understanding electrochemically switchable rotaxanes and opens up new possibilities for their potential applications in various fields.

In 2020, Shahraki Bahareh Taghavi and colleagues[26], are focused on developing new and innovative methods for synthesizing mechanically interlocked molecules like rotaxanes and catenanes. These molecules include mobile rings that slide along an axis within another molecule or mechanically interlock with another molecule. The study delved into the new techniques and methods applied to efficiently and precisely prepare these mechanically interlocked molecules. This contributes to expanding the potential applications of these molecules in various fields, including chemistry and materials science .Overall, this study sheds light on advancements in the synthesis of mechanically interlocked molecules and provides new and innovative approaches for their use in diverse scientific research and applications.

In 2021[27], Barclay Matthew S. and colleagues are conducted a study focused on the use of rotaxane rings in the context of DNA-templated molecular dye aggregates. The researchers investigated how these rotaxane rings influence the packing and lifetimes of molecular dye aggregates when guided by DNA templates .The results of the study revealed that the presence of rotaxane rings promotes oblique packing and extends the lifetimes of the molecular dye aggregates. This finding has implications for the design of molecular assemblies guided by DNA templates, potentially enhancing their stability and functionality .In summary, this study highlights the role of rotaxane rings in influencing the arrangement and stability of DNA-templated molecular dye aggregates, offering insights into the development of novel molecular structures with potential applications in various fields.

In 2022 [28], Wu Peiqiao and colleagues are conducted a comprehensive assessment of the use of rotaxane nanomachines in future molecular electronics. In this study, they ventured into the field of nanotechnology and molecular interactions at the nanoscale.The study provided an overview of how to design and utilize rotaxane nanomachines in molecular electronics and explored their potential applications in areas such as information storage, nanodevices, and quantum computing. It also reviewed the challenges facing this field and anticipated future developments.In summary, this study offered a comprehensive insight into the potential use of rotaxane nanomachines in the field of molecular electronics and contributed to directing research towards promising future applications in nanotechnology.

In 2023[29], Jana Gourhari and Mendoza-Cortes are published a first-principles molecular dynamics study was conducted to delve into the

thermodynamics, kinetics, and optical properties of rotaxane. This research aimed to provide a deeper understanding of the behavior and characteristics of rotaxane molecules at the molecular level. The study investigated the thermodynamic aspects, such as energy changes, and the kinetics, which involve the rates of processes, related to rotaxane molecules. Additionally, it explored the optical properties, shedding light on how these molecules interact with light and their potential applications in optics and photonics. Overall, this research contributed to advancing our knowledge of rotaxane molecules' behavior and properties through computational simulations, offering valuable insights for potential applications in various scientific fields.

Ata Utku zkan *et al*, in 2023 [30], have demonstrated the effect of charge state on the equilibrium and Kinetic properties of mechanically interlocked Rotaxane. Their theoretical investigation predicates that the Rotaxanes can respond to stimuli by permitting positional changes in their rota groups in reaction to physiochemical conditions like variations in solution pH.

1.5. The Aim of the Study

The aim of this work is studied by investigates some of goals:

1. The invistagation of structural, morphological, electronic, electric and thermoelectric charcteristics of a series of Rotaxane molecular junctions.
2. Obtain a deep understanding of fundamental conceptes such as the quantum size effect and their impact on the characteristics of molecular systems under investigation in this work.
3. The conclusion and predications of the possible applications of this kind of molecular nanojuctions, such as the electronic and optoelectronics.

2.1. Introduction

DFT is widely used by physicists and chemists to investigate the ground-state properties of interacting many-particles systems such as atoms, molecules and crystals. DFT transforms the many-body system into one of non-interacting fermions in an effective field. In other words, the electrical properties of many interacting particles system can be described as a functional of the ground-state density of the system [31]. In 1998, the importance of DFT was confirmed with the Nobel Prize in Chemistry being awarded to Walter Kohn for his development of density functional theory. DFT is a reliable methodology which has been applied to a large variety of molecular systems with a huge number of books and articles in the literature giving detailed descriptions of the principles of DFT and its application [32]. The beginnings of DFT were founded upon the Thomas-Fermi model back in the 1920s which provided the basic steps to obtain the density functional for the total energy based on wavefunctions [31,33] Further improvement was made by Hartree, Dirac, Fock and Slater and nearly four decades after the Thomas-Fermi work. DFT was then given a robust foundation by the Hohenberg-Kohn theorems and Kohn-Sham method [31, 33,34].

The main aim of this chapter is to give brief introduction to DFT and outlining the main formalism as a method of finding the solution of the non-relativistic many-particles time independent Schrödinger equation TISE, since the properties of a many-electron system can be determined by using functionals of the electron density. I will also give a brief summary of the DFT code ‘SIESTA’ which I have used extensively throughout my PhD research as a theoretical tool to optimise the structures.

2.2. Schrödinger Equation and Variational Principle

Any given non-relativistic many particles system can be described by the time independent, non-relativistic Schrödinger equation[35]:

$$\mathrm{H}\Psi_i(\vec{r}_1,\vec{r}_2,\dots,\vec{r}_N,\vec{R}_1,\vec{R}_2,\dots,\vec{R}_M) = E_i\Psi_i(\vec{r}_1,\vec{r}_2,\dots,\vec{r}_N,\vec{R}_1,\vec{R}_2,\dots,\vec{R}_M) \quad (2.1)$$

here H represents the Hamiltonian operator of a system consisting of *N*-electrons and *M*-nuclei which describes the interaction of particles with each other, where Ψ_i is the wavefunction of the i^{th} state of the system and E_i is the numerical value of the energy of the i^{th} state described by Ψ_i. The Hamiltonian operator of such a system can be written as a sum of five terms given by [36,37]:

$$\begin{aligned}\mathrm{H} = &\overbrace{-\frac{\hbar^2}{2m_e}\sum_{i=1}^{N}\nabla_i^2}^{T_e} - \overbrace{\frac{\hbar^2}{2m_n}\sum_{n=1}^{M}\nabla_n^2}^{T_n} - \overbrace{\frac{1}{4\pi\varepsilon_o}\sum_{i=1}^{N}\sum_{n=1}^{M}\frac{1}{\left|\vec{r}_i-\vec{R}_n\right|}Z_n e^2}^{U_{en}} \\ &+ \frac{1}{4\pi\varepsilon_o}\frac{1}{2}\overbrace{\sum_{i=1}^{N}\sum_{i\neq j}^{N}\frac{e^2}{\left|\vec{r}_i-\vec{\vec{r}}_j\right|}}^{U_{ee}} \\ &+ \overbrace{\frac{1}{4\pi\varepsilon_o}\frac{1}{2}\sum_{n=1}^{M}\sum_{n\neq n'}^{M}\frac{1}{\left|\vec{R}_n-\vec{R}_{n'}\right|}Z_n Z_{n'}e^2}^{U_{nn}}\end{aligned} \quad (2.2)$$

here i and j denote the *N*-electrons while n and n' run over the *M*-nuclei in the system, m_e and m_n are the mass of electron and nucleus respectively, e and Z_n are the electron and nuclear charge respectively. The position of the electrons and nuclei are denoted as $\vec{r}_i$ and $\vec{R}_n$ respectively, and ∇_i^2 is the Laplacian operator, in Cartesian coordinates ∇_i^2 is defined as:

$$\nabla_i^2 = \frac{\partial^2}{\partial x_i^2} + \frac{\partial^2}{\partial y_i^2} + \frac{\partial^2}{\partial z_i^2}$$

In the equation (2.2), the first and two terms, T_e and T_n represent the kinetic energy of electrons and nuclei respectively. The last three terms represent the potential part of the Hamiltonian; where U_{en} defines the attractive electrostatic interaction between electrons and nuclei. The electron-electron,U_{ee} and nuclear-nuclear, U_{nn} describe the repulsive part of the potential respectively [31, 34, 32].

The Born-Oppenheimer approximation, also called the clamped nuclei approximation can be applied due to the fact that is about 99.9% of atom's mass is concentrated in the nucleus (for example, the hydrogen nucleus weighs approximately 1800 times more than an electron) and the nuclei can be considered fixed as compared to the electrons. In this case, if the nuclei of the treated atoms are fixed, their kinetic energy is zero and they do not contribute to the full wavefunction anymore. The outcome of this assumption is that the Hamiltonian of the electron system reduces the Hamiltonian to a new one, the electronic Hamiltonian H_{ele} which in the fixed nuclear picture can be rewritten as [31, 34,38]:

$$\mathrm{H}_{ele} = \overbrace{-\frac{\hbar^2}{2m_e}\sum_{i=1}^{N}\nabla_i^2}^{T_e} \overbrace{-\frac{1}{4\pi\varepsilon_o}\sum_{i=1}^{N}\sum_{n=1}^{M}\frac{1}{\left|\vec{r}_i - \vec{R}_n\right|}Z_n e^2}^{U_{en}} + \overbrace{\frac{1}{4\pi\varepsilon_o}\frac{1}{2}\sum_{i=1}^{N}\sum_{i\neq j}^{N}\frac{e^2}{\left|\vec{r}_i - \vec{r}_j\right|}}^{U_{ee}} \quad (2.3)$$

where U_{nn} is a determined constant. For such a system, the Schrödinger equation for 'clamped-nuclei' is:

$$\mathrm{H}_{ele}\Psi_{ele} = E_{ele}\Psi_{ele} \qquad (2.4)$$

where Ψ_{ele} depends on the electron coordinates, while the nuclear part enters only parametrically and does not explicitly appear in Ψ_{ele}. The total energy E_{total} is then the sum of E_{ele} and the constant nuclear repulsion term which is given by:

$$E_{total} = E_{ele} + U_{nn} \qquad (2.5)$$

The wavefunction itself is not an observable quantity while its modulus squared can be written as:

$$|\Psi(\vec{r}_1, \vec{r}_2, \dots, \vec{r}_N)|^2 d\vec{r}_1\, d\vec{r}_2 \dots d\vec{r}_N \qquad (2.6)$$

which represents the probability that electrons 1,2,…..,*N* are found in the volume elements $d\vec{r}_1\, d\vec{r}_2 \dots\dots d\vec{r}_N$, since electrons are indistinguishable, this probability is unchangeable if the coordinates of any two electrons (here *i* and *j*) are swapped [36]:

$$\left|\Psi(\vec{r}_1, \vec{r}_2, \dots \vec{r}_i, \vec{r}_j, \dots, \vec{r}_N)\right|^2 = \left|\Psi(\vec{r}_1, \vec{r}_2, \dots \vec{r}_j, \vec{r}_i, \dots, \vec{r}_N)\right|^2 \qquad (2.7)$$

Due to fact that electrons are fermions with spin of a half then Ψ must therefore be antisymmetric with respect to the interchange of the spatial and the spin coordinates of any two electrons:

$$\Psi\left(\vec{r}_1, \vec{r}_2, \dots \vec{r}_i, \vec{r}_j, \dots, \vec{r}_N\right) = -\Psi\left(\vec{r}_1, \vec{r}_2, \dots \vec{r}_i, \vec{r}_j, \dots, \vec{r}_N\right) \qquad (2.8)$$

A logical consequence of the probability interpretation of the wavefunction is that the integral of equation (2.6) over the full range of all variables equals one. In other words, the probability of finding the *N*-electron anywhere in space must be exactly unity,

$$\int \dots \int |\Psi(\vec{r}_1, \vec{r}_2, \dots, \vec{r}_N)|^2 \, d\vec{r}_1 \, d\vec{r}_2 \dots d\vec{r}_N = 1 \qquad (2.9)$$

A wavefunction which satisfies equation (2.9) is a normalized wavefunction. Since there is no exact solution of the Schrödinger equation, many theories have been developed to achieve this goal; it began from Hartree, Hartree-Fock and others. Most of these theories were based on an important theoretical principle called the variational principle of the wavefunction [31, 36]. Simply, this principle informs us how to look for solutions by using suitable trial wavefunctions Ψ_{Tri}. This principle is useful to study the ground state, but is not very useful for the study of excited states. When a system is in the state Ψ_{Tri}, the expectation value of the energy is given by [31, 34]:

$$\langle E_{Tri} \rangle = \frac{\int \Psi_{Tri} \, \mathrm{H} \, \Psi^*_{Tri} \, d\vec{r}}{\int \Psi_{Tri} \; \Psi^*_{Tri} \, d\vec{r}} \qquad (2.10)$$

The variational principle appears in equation (2.10). This means that the energy computes as the expectation value of the Hamiltonian operator from any Ψ_{Tri} (guessed wavefunction) which is an upper bound to the true ground-state energy Ψ_{GS}. If Ψ_{Tri} is normalized according to equation (2.9), and Ψ_{Tri} equals to the ground state ($\Psi_{Tri} = \Psi_{GS}$). This means E_{Tri} equals to the exact ground state energy E_{GS}, now equation (2.10) can be rewriten for the ground state as:

$$\langle E_{GS} \rangle = \int \Psi_{GS} \, \mathrm{H} \, \Psi_{GS}^{*} \, d\vec{r} \tag{2.11}$$

The normalized Ψ_{Tri} can show that $E_{Tri} > E_{GS}$ or $E_{Tri} = E_{GS}$. Therefore the best choice of E_{Tri} is the one in which E_{Tri} is minimized [33,34].

2.3. The Hohenberg-Kohn Theorems

DFT is based on Hohenberg-Kohn theorems; which in 1964, Hohenberg and Kohn legitimized the use of the electron density $n(\vec{r})$ to calculate the ground state energy [39,40]:

Theorem (1), states that for any interacting many particle system with an applied external potential$V_{ext}(\vec{r})$, the density is uniquely determined. In other words, it demonstrates that the density $n(\vec{r})$ may be used instead of the potential as a basic function uniquely characterising the system, and be stated as the ground state density $n_{GS}(\vec{r})$ which uniquely determines the potential up to an arbitrary constant [41,42].

Proof (1), originally, in their paper, this theorem is proven for densities with non-degenerate ground states and the proof is elementary and by contradiction [43]. Let us consider two different external potentials $V_{ext}(\vec{r})_{(1)}$and $V_{ext}(\vec{r})_{(2)}$ which differ by more than a constant and yield the same ground state density $n_{GS}(\vec{r})$. Clearly the above two potentials correspond to distinct Hamiltonians which are $H_{ext}[(\vec{r})]_{(1)}$ and $H_{ext}[(\vec{r})]_{(2)}$, these Hamiltonians give rise to distinct wavefunctions which are $\Psi_{ext}[(\vec{r})]_{(1)}$ and $\Psi_{ext}[(\vec{r})]_{(2)}$.

Since we have the same ground state and according to the variational principle which tell us that there is no wavefunction that gives energy less than the energy of $\Psi_{ext}[(\vec{r})]_{(1)}$ for $H_{ext}[(\vec{r})]_{(1)}$, that is:

$$\langle E_{(1)} \rangle = \int \Psi_{(1)}\, H_{(1)}\, \Psi^*_{(1)}\; d\vec{r} < \int \Psi_{(2)}\, H_{(2)}\, \Psi^*_{(2)}\; d\vec{r} \qquad (2.12)$$

For non-degenerate ground state and because of the identical ground state densities for two Hamiltonians, the equation (2.12) becomes:

$$\begin{aligned} &\int \Psi_{(2)}\, H_{(1)}\, \Psi^*_{(2)}\; d\vec{r} \\ &= \overbrace{\int \Psi_{(2)}\, H_{(2)}\, \Psi^*_{(2)}\; d\vec{r}}^{\langle E_{(2)} \rangle} \\ &+ \int \left\{ [V_{ext}(\vec{r}\,)]_{(1)} \right. \\ &\left. - [V_{ext}(\vec{r}\,)]_{(2)} \right\} n_{GS}(\vec{r})\, d\vec{r} \end{aligned} \qquad (2.13)$$

By exchanging the labels in equation (2.13), we have:

$$\begin{aligned} &\int \Psi_{(1)}\, H_{(2)}\, \Psi^*_{(1)}\, d\vec{r} = \\ &= \overbrace{\int \Psi_{(1)}\, H_{(1)}\, \Psi^*_{(1)}\; d\vec{r}}^{\langle E_{(1)} \rangle} \\ &+ \int \left\{ [V_{ext}(\vec{r}\,)]_{(2)} - [V_{ext}(\vec{r}\,)]_{(1)} \right\} n_{GS}(\vec{r})\, d\vec{r} \end{aligned} \qquad (2.14)$$

Adding the equations (2.13) and (2.14) we obtain:

$$\langle E_{(1)} \rangle + \langle E_{(2)} \rangle < \langle E_{(2)} \rangle + \langle E_{(1)} \rangle \qquad (2.15)$$

Clearly,equation (2.15) shows a contradiction. Thus, the theorem has been proven by reductio ad absurdum.

Theorem (2), provides a variational ansatz for obtaining $n(\vec{r})$, i.e. searching for $n(\vec{r})$ which minimises the energy. In other words, it states that, in terms of the density $n(\vec{r})$, we can define a universal functional for the energy $E[n(\vec{r})]$. The exact ground state energy of the system in particular ($V_{ext}(\vec{r})$) is the global minimum value of this functional and the density $n(\vec{r})$ which minimizes the functional and represents the exact ground state density $n_{GS}(\vec{r})$ [43,44].

Proof (2), the first theorem tells us that the total energy of the system is as a functional of the density $n(\vec{r})$ and is given by:

$$E_{total}[n(\vec{r})] = \overbrace{T_{int}[n(\vec{r})] + \underbrace{U_{ee}[n(\vec{r})]}_{\substack{=zero,\ for\\ non-interacting\\ system}}}^{F_{H-K}[n(\vec{r})]} + \int V_{ext}(\vec{r})\ n(\vec{r})\ d\vec{r} \tag{2.16}$$

The first two terms in equation (2.16) ($F_{H-K}[n(\vec{r})]$) are the kinetic energy (T_{int}) and the electron-electron interaction energy (U_{ee}) is treated as the same for the whole system. Thus $F_{H-K}[n(\vec{r})]$ is a universal functional, it has been described as the Holy Grail of density functional theory [36]. Assuming that the system is in the ground state, we can define the energy uniquely by the ground state density $n_{GS}(\vec{r})$ as:

$$\langle E_{GS}\rangle = \langle E[n_{GS}(\vec{r})]\rangle = \int \Psi_{GS}\, H_{GS}\, \Psi^{*}_{GS}\ d\vec{r} \tag{2.17}$$

According to the variational principle, the ground state energy which corresponds to the ground state density is the minimum energy and any different density will necessarily provide a higher energy:

$$\langle E_{GS} \rangle = \langle E[n_{GS}(\vec{r})] \rangle = \int \Psi_{GS} \, H_{GS} \, \Psi_{GS}^{*} \; d\vec{r}$$

$$< \int \Psi \, H \, \Psi^{*} \; d\vec{r} \quad = \langle E[n(\vec{r})] \rangle \quad = \langle E \rangle \tag{2.18}$$

Once we know the functional $F_{H-K}[n(\vec{r})]$, the total energy can be minimized with respect to variations in the density function in the equation (2.16), that leads to finding the exact ground state properties of the system that we are looking for (we should take into account that for most practical calculations, the direct minimization will not provide us the ground state energy, but by the simpler procedure due to Kohn-Sham).

2.4. Kohn-Sham Method and Self-Consistent Field

Kohn and Sham noticed that Hohenberg-Kohn theory is applicable to both interacting and non-interacting systems. As DFT avoids the interacting many particle problem. The non-interacting system has one great advantage over the interacting system as finding the ground-state energy for a non-interacting system is easier. In 1965, Kohn and Sham came up with the idea, that it is possible to replace the original Hamiltonian of the system by an effective Hamiltonian (H_{eff}) of the non-interacting system in an effective external potential $V_{eff}(\vec{r})$ which gives rise to the same ground state density as the original system. Since there is no clear recipe for calculating this, the Kohn-Sham method is considered as an ansatz, but it is considerably easier to solve than the non-interacting

problem. The Kohn-Sham method is based on the Hohenberg-Kohn universal density [44]:

$$F_{H-K}[n(\vec{r})] = T_{int}[n(\vec{r})] + U_{ee}[n(\vec{r})] \tag{2.19}$$

The Hohenberg-Kohn functional for non-interacting electrons is reduced to only the kinetic energy. The energy functional of the Kohn-Sham ansatz $F_{K-S}[n(\vec{r})]$, in contrast to (2.16), is given by:

$$F_{K-S}[n(\vec{r})] = T_{non}[n(\vec{r})] + E_{Hart}[n(\vec{r})] + \int V_{ext}(\vec{r})\ n(\vec{r})\, d\vec{r} + E_{xc}[n(\vec{r})] \tag{2.20}$$

where T_{non} is the kinetic energy of the non-interacting system which is different than T_{int} (for interaction system) in equation (2.16), while E_{Hart} is the classical electrostatic energy or classical self-interaction energy of the electron gas which is associated with density $n(\vec{r})$. The fourth term E_{xc} is the exchange-correlation energy functional and given by:

$$E_{xc}[n(\vec{r})] = F_{H-K}[n(\vec{r}) - \overbrace{\frac{1}{2}\int \frac{n(\vec{r}_1)n(\vec{r}_2)}{|\vec{r}_1 - \vec{r}_2|} d\vec{r}_1 d\vec{r}_2}^{E_{Hart}[n(\vec{r})]} - T_{non}[n(\vec{r})] \tag{2.21}$$

The first, second and third terms in the equation (2.20) can be trivially cast into functional form. In contrast, there is in general no exact functional form for E_{xc}. In the last couple of decades, enormous efforts have gone into finding a better approximation toE_{xc}. Currently, the functionals can investigate and predict the physical properties of a wide range of solid state systems and molecules. For the last three terms in the equation (2.20), we take the functional derivatives to construct the effective single particle potential $V_{eff}(\vec{r})$:

$$V_{eff}(\vec{r}) = V_{ext}(\vec{r}) + \frac{\partial E_{Hart}[n(\vec{r})]}{\partial n(\vec{r})} + \frac{\partial E_{xc}[n(\vec{r})]}{\partial n(\vec{r})} \quad (2.22)$$

Now, this potential can be used to give the Hamiltonian of the single particle:

$$H_{K-S} = T_{non} + V_{eff} \quad (2.23)$$

By using this Hamiltonian, the Schrödinger equation becomes:

$$[T_{non} + V_{eff}]\Psi_{K-S} = E\Psi_{K-S} \quad (2.24)$$

Equation (2.24) is known as Kohn-Sham equation. The ground state density $n_{GS}^{K-S}(\vec{r})$ corresponds to the ground state wavefunction Ψ_{GS}^{K-S} which by definition minimizes the Kohn-Sham functional subject to the orthonormalization constraints $\langle\Psi_i|\Psi_j\rangle = \delta_{ij}$; it is found by a self-consistent calculation [40,45].

Density functional theory uses a self-consistent field procedure. For example, let us suppose that E_{Hart} and E_{xc} can be accurately determined. The problem is now that V_{eff} cannot be calculated until the correct ground state density is known and the correct density cannot be obtained from the Kohn-Sham wavefunctions until equation (2.24) is solved with the correct V_{eff}. Therefore this circular problem is solved by carrying out a self-consistent cycle [46, 47] as shown in Figure 2.1.

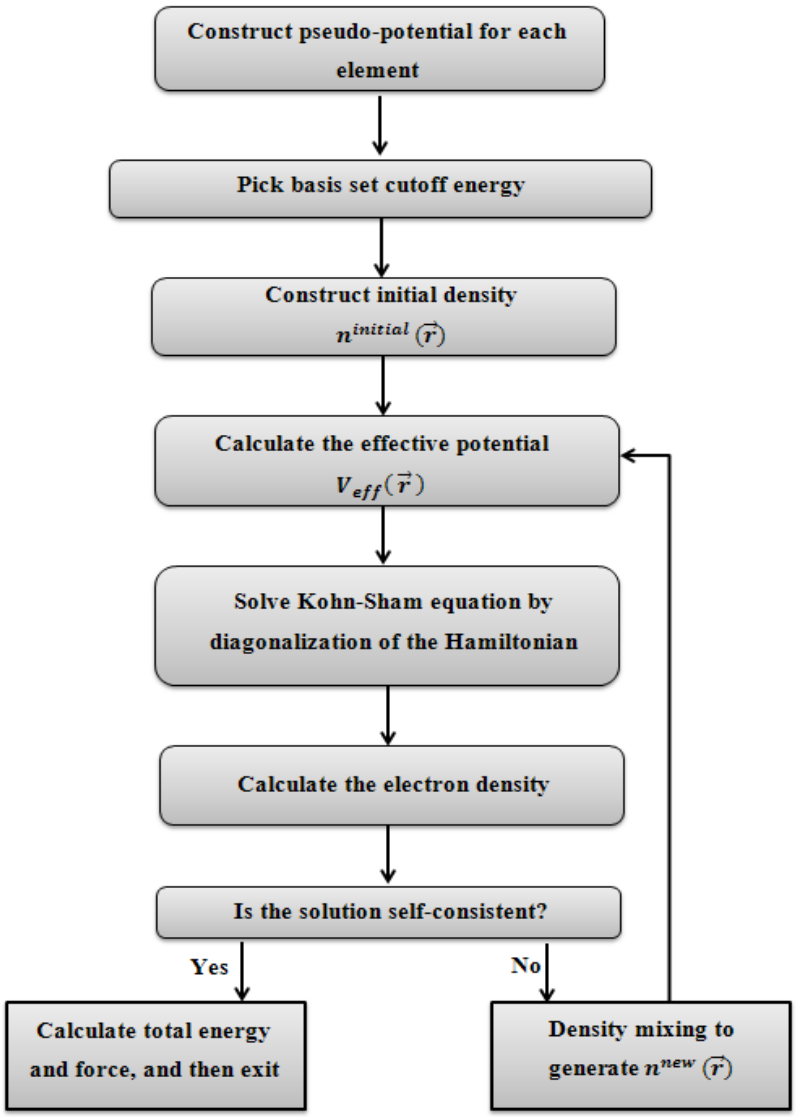

Figure 2.1. A Schematic Illustration of the Self-consistent DFT Cycle.

According to Figure 2.1, the first step is to generate the pseudo-potential which represents the electrostatic interaction between the valence electrons and the nuclei and core electrons. The next step is to build the required basis set with a selected kinetic energy cutoff to be inserted in the basis set; this step is to expand the density functional quantities. Clearly, if the density is known, the energy functional is fully determined. A trial electronic density $n^{initial}(\vec{r})$ is made as an initial guess. This initial guess is used to calculate the following quantity:

$$G = E_{Hart}[n^{initial}(\vec{r})] + E_{xc}[n^{initial}(\vec{r})] \qquad (2.25)$$

Then $\frac{\partial G}{\partial n^{initial}(\vec{r})}$ and the effective potential V_{eff} are calculated. The effective potential is used to solve the Kohn-Sham equation (2.24) which leads to finding the electron Hamiltonian. After obtaining the Hamiltonian, it is diagonalised in order to find the eigenfunctions and the new electron density $n^{new}(\vec{r})$. Hopefully, this $n^{new}(\vec{r})$ will be closer to true ground state and is checked. For self-consistency, if this new updated electron density $n^{new}(\vec{r})$ agrees numerically with the density $n^{initial}(\vec{r})$ used to build the Hamiltonian at the beginning of the SCF cycle, we have reached the end of the loop. We then exit, and calculate all the desired converged quantities, such as the total energy, the electronic band structure, density of states, *etc*... Otherwise, the new density $n^{new}(\vec{r})$ does not agree with the starting density $n^{initial}(\vec{r})$, one generates a new input density and starts another SCF cycle: build the new density-dependent Hamiltonian, solve and compute the density, and check for self-consistency [32,40,48].

The Kohn-Sham approach clearly shows that a complicated many body system can be mapped onto a set of simple non-interacting equations exactly if the exchange correlation functional is known. However, the exchange-correlation functional is not known exactly so approximations need to be made.

2.5. The Exchange-Correlation Potential

DFT is very reliable and proven method, but it still uses an approximation for the kinetic energy functional and the exchange-correlation functional in terms of the density. Huge efforts have been aimed at finding reliable expressions for those functionals. The most commonly exchange-correlation functional approximations are the Local Density Approximation (LDA), which depends only on the density, and the more

complicated Generalised Gradient Approximation (GGA), which includes the derivative of the density and also contains information about the environment and hence it is semi-local[49].

2.5.1. Local Density Approximation (LDA)

Based on Kohn-Sham method, the functional E_{xc} functional could be calculated in a homogenous electron gas to approximate the many body particle problem as a simpler system [39]. Kohn-Sham demonstrated that by slowly varying the density of a system, the E_{xc} functional at point $\vec{r}$ can be considered as acting in a uniform density. Therefore the E_{xc} functional can be represented by a uniform electron gas $E_{xc}^{homo}[n(\vec{r})]$ with a density $n(\vec{r})$.

In general the LDA will not work for systems which are dominated by electron-electron interactions. However, LDA supposes that the density is a constant in the local region around any considered position and it is given by [46]:

$$E_{xc}^{LDA}[n(\vec{r})] = \int E_{xc}^{homo}[n(\vec{r})]n(\vec{r})d\vec{r} \qquad (2.26)$$

The exchange-correlation energy $E_{xc}^{homo}[n(\vec{r})]$ can be split into two terms as the sum of the exchange $E_{x}^{homo}[n(\vec{r})]$ and the correlation energies $E_{c}^{homo}[n(\vec{r})]$ which can be found separately as:

$$E_{xc}^{homo}[n(\vec{r})] = E_{x}^{homo}[n(\vec{r})] + E_{c}^{homo}[n(\vec{r})] \qquad (2.27)$$

The exchange term can be found analytically; it is well known and can be found in many textbooks (see [32, 36]) and it is given by:

$$E_{x}^{homo}[n(\vec{r})] = -\frac{3}{4}\left(\frac{3n(\vec{r})}{\pi}\right)^{1/3} \qquad (2.28)$$

The correlation energy ($E_c^{homo}[n(\vec{r})]$) term cannot be obtained analytically, but it can be calculated accurately using numerical methods. The most common and accurate method was proposed by **C**eperly and **A**lder **(CA)** [50] using quantum Monte-Carlo simulations. There are several different interpretations of the Monte Carlo data, for example, the most used was calculated by **P**erdew and **Z**unger (PZ), who fitted this numerical data to an analytical expression and obtained [46,51]:

$$\boldsymbol{E_c^{homo}[n(\vec{r})]} \begin{cases} -0.048 + 0.031\, ln(r_o) - 0.0116\, r_o + 0.002\ ln(r_o) & if\ r_o < 1 \\ -\frac{0.1423}{(1+1.9529\sqrt{r_o}+0.3334\, r_o} & if\ r_o > 1 \end{cases} \quad (2.29)$$

here r_o is the average radius of the electrons in the homogenous electron gas and defined as $(\frac{3}{4\pi n})^{1/3}$.

The LDA is a simple and well known powerful functional, it is considered to be accurate for graphene and carbon nanotubes or where the electron density is not rapidly changing. A larger error is expected for atoms with *d* and *f* orbitals. This functional to some extent has many pitfalls, for example the band gap in semiconductors and insulators is usually not accurate with a large error (in the range of 0.5 to 2eV or 10-30%). For this reason it is highly advisable to seek better functionals [47, 51,52].

2.5.2. Generalized Gradient Approximation (GGA)

LDA treats all systems as the homogenous systems, but the real systems are inhomogeneous. In order to take this into account, a step may be taken beyond the LDA and extend it by including the derivative information of

the density into the exchange-correlation functionals. The only way to do this, is by including the gradient and the higher spatial derivatives of the total charge density ($|\nabla n(\vec{r})|, |\nabla^2 n(\vec{r})|, ...$) into the approximation. Such a functional is called the generalized gradient approximation (GGA). For this case, there is no closed expression for the exchange part of the functional and therefore it has to be calculated along with the correlation contributions using numerical methods. Exactly as in the case of the LDA many parameterizations exist for the exchange-correlation energies in the GGA [51].

In this section, we are going to discuss the proposed functional form which is presented by **P**erdew, **B**urke and **E**rnzerhof (PBE) [51]. In this parameterization, there are two separated expressions, the first expression is the exchange $E_x^{GGA}[n(\vec{r})]$ and given by:

$$E_x^{GGA}[n(\vec{r})] = \int n(\vec{r})\, E_x^{homo}[n(\vec{r})]\; F_x(s) d\vec{r}\,, \qquad (2.30)$$

$$F_x(s) = 1 + \kappa - \frac{\kappa}{(1+\mu s^2)/\kappa}$$

here $F_x(s)$ is called the enhancement factor, $\kappa = 0.804$, $\mu = 0.21951$ and $s = |\nabla n(\vec{r})/2k_s n(\vec{r})|$ is the dimensionless density gradient, where $k_s = \sqrt{\frac{4\, k_{T-F}}{\pi a_o}}$ and $k_{T-F} = \frac{(12/\pi)^{1/3}}{\sqrt{r_s}}$ is the Thomas-Fermi screening wavenumber whereas r_s is the local Seitz radius.

The second expression is the correlation energy $E_x^{GGA}[n(\vec{r})]$ and given by:

$$E_c^{GGA}[n(\vec{r})] = \int (E_c^{homo}[n(\vec{r})] + \chi\,[n(\vec{r})]) d\vec{r}\,, \qquad (2.31)$$

$$\chi\,[n(\vec{r})] = \frac{e^2}{a_o}\,\gamma\, ln\left(1 + \frac{\beta}{\gamma}\, t^2\, \frac{1+At^2}{1+At^2+A^2t^4}\right),$$

$$A = \frac{\beta}{\gamma}\left[e^{\left(\frac{E_C^{homo}[n(\vec{r})]}{\gamma}\right)^{-1}} \right]^{-1}$$

where $\gamma = (1 - ln(2)/\pi^2$, $t = |\nabla n(\vec{r})/2k_{T-F}n(\vec{r})|$ is another dimensionless density gradient, $\beta = 0.066725$, and $a_0 = \frac{\hbar}{me^2}$.

LDA and GGA are the two most commonly used approximations for the approximation of exchange-correlation energies in the DFT. Also, there are several other functionals, which go beyond LDA and GGA. In general, there is no robust theory of the validity of these functionals. It is determined via testing the functional for various materials over a wide range of systems and comparing results with reliable experimental data.

2.6. SIESTA

All calculations in this thesis were carried out by the implementation of DFT in the SIESTA code. It is used to obtain the relaxed geometry of the discussed structures and also to carry out the calculations to investigate their electronic properties. SIESTA is an acronym derived from the *S*panish *I*nitiative for *E*lectronic *S*imulations with *T*housands of *A*toms. It is a self-consistent density functional theory technique which uses norm-conserving pseudo-potentials and a **L**inear **C**ombination of **A**tomic **O**rbital **B**asis **s**et (LCAOBs) to perform efficient calculations [53]. For more theoretical details about SIESTA code and what it provides in, see [54]. There are two different modes to perform DFT simulations using SIESTA one a conventional self-consistent field diagonalisation method to solve the Kohn-Sham equations and two by direct minimization of a modified energy functional [55]. This section will describe some of SIESTA's components and how they are implemented within the code.

2.6.1. Localised Atomic Orbital Basis Sets (LAOBs)

One of the most important aspects of the SIESTA code is the type of the basis function employed in the calculations. It uses a basis set composed of localised atomic orbitals which compare well with other DFT schemes which may use a plane wavefunction basis set [56]. The benefits from using LAOBs are that they provide a closer representation of the chemical bond; they can allow order-N calculations to be performed and also it gives a good base from which generate a tight-binding Hamiltonian. SIESTA uses confined orbitals, i.e. orbitals are constrained to be zero outside of a certain radius (cutoff radius r_c). This produces the desired sparse form of the Hamiltonian as the overlap between basis functions is reduced. The atomic orbitals inside this radius are products of a numerical radial function and a spherical harmonic.

The simplest form of the atomic basis set for an atom (labelled as I) is called single-ζ (also called minimal) which represents a single basis function per electron orbital. It is given by the following equation:

$$\Psi^{\mathrm{I}}_{nlm}(\vec{r}) = R^{\mathrm{I}}_{nl}(\vec{r})\, Y^{\mathrm{I}}_{lm}(\vec{r}) \qquad (2.32)$$

where $\Psi^{\mathrm{I}}_{nlm}(\vec{r})$ is the single basis function which consists of two parts, the first part is the radial wavefunction R^{I}_{nl} and the second part is the spherical harmonic Y^{I}_{lm}. Minimal or single zeta basis set are constructed by using one basis function of each type occupied in the separate atoms that comprise a molecule. If at least one *p-type* orbital is occupied in the atom, then the complete set (*3p-type*) of the functions must be included in the basis set. For example, in the carbon atom, the electron configuration is $1s^2\ 2s^2\ 2p^2$, therefore, a minimal basis set for carbon atom consists of $1s, 2s, 2p_x, 2p_y$ and $2p_z$ orbitals which means the total basis functions are five as shown in Table 2.1.

Higher accuracy basis sets called multiple-ζ are formed by adding another radial wavefunctions for each included electron orbital. Double basis sets are constructed by using two basis functions of each type for each atom. For carbon atom, a double zeta basis contains ten basis functions corresponding to ten orbitals which are $1s, 1s', 2s, 2s', 2p_x, 2p'_x, 2p_y, 2p'_y,$ $2p_z$ and $2p'_z$. For further accuracy, polarisation effects are included in double-ζ polarised basis sets obtained by including wavefunctions with different angular momenta corresponding to orbitals which are unoccupied in the atom. A polarization function is any higher angular momentum orbital used in a basis set which is unoccupied in the separated atom. As an example, the hydrogen atom has only one occupied orbital type that is *s*-type. Therefore, if *p*-type or *d*-type basis functions were added to the hydrogen atom they would be known as polarization functions. Carbon atoms with polarization functions include *d*-type and *f*-type basis functions.

Table 2.1. Examples of the radial basis sets functions per atom used in SIESTA code for different precisions of the split valence basis sets [57].

Atom/Basis Functions	Single-ζ (SZ)	Double-ζ (DZ)	Single-ζ Polarised (SZP)	Double-ζ Polarised (DZP)
$H^1/1s$	1	2	4	5
$C^6/1s\ 2s\ 2p_x 2p_y 2p_z$	4	8	9	13
$N^7/1s\ 2s 2p_x 2p_y 2p_z$	4	8	9	13

Assuming the core electrons (non-valence electrons) of an atom are less affected by the chemical environment than the valence electrons. This is so-called as split valence basis set. For example, the carbon atom, a split valence double zeta basis set would consist of a single $1s$ orbital, along

with $2s, 2s'$and $2p_x, 2p'_x, 2p_y, 2p'_y,\ 2p_z, 2p'_z$ orbitals, for a total of 9 basis functions. The basis functions in a split valence double zeta basis set are denoted $1s, 2s, 2s', 2p_x, 2p'_x, 2p_y, 2p'_y,\ 2p_z, 2p'_z$. In case of molecules, molecular orbitals can be represented as Linear Combinations of Atomic Orbitals (LCAO-MO) given by:

$$\varphi_i(\vec{r}) = \sum_{\upsilon=1}^{L} a_{\upsilon i}\ \Psi_\upsilon(\vec{r}) \tag{2.33}$$

where φ_i represents the molecular orbitals (basis functions), Ψ_υ are atomic orbitals, $a_{\upsilon i}$ are numerical coefficients and L is the total number of the atomic orbitals.

2.6.2. Basis Set Superposition Error Correction (BSSE)

The Basis Set Superposition Error Correction (BSSE) is one of the major factors affecting the accuracy of interaction energy calculations when using incomplete basis sets. It is most often discussed in the context of intermolecular interactions and frequently for weakly interacting systems. The SIESTA implementation of DFT used in this thesis means that the BSSE occurs when using the linear combination of the atomic orbitals formalism which consists of a finite basis set centred on the nuclei, when atoms are close enough to each other so that their basis functions will overlap. This might cause artificial strengthening of the atomic interaction and artificial shortening of the atomic distances and therefore this can affect the total energy of the system. In 1970, Boys and Bernardi proposed a technique to eliminate the BSSE in molecular complexes composed of two geometric configurations so-called the counterpoise correction (CP) scheme [58]. Let us consider two molecular systems which are labelled as A and B. They are separated by a distance R. The energy of the interaction may be expressed as [59]:

$$\Delta E_{inter}^{AB}(\vec{R}) = E^{AB}(\vec{R}) - E^{A} - E^{B} \qquad (2.34)$$

where ΔE_{inter}^{AB} is the overall energy of the supersystem, $E^{A}$and E^{B} are the energies of the isolated subsystems. The form of equation 2.34 shows the counterpoise correction [58]. Figure 2.3 highlights the counterpoise correction for a dimer which are A and B.

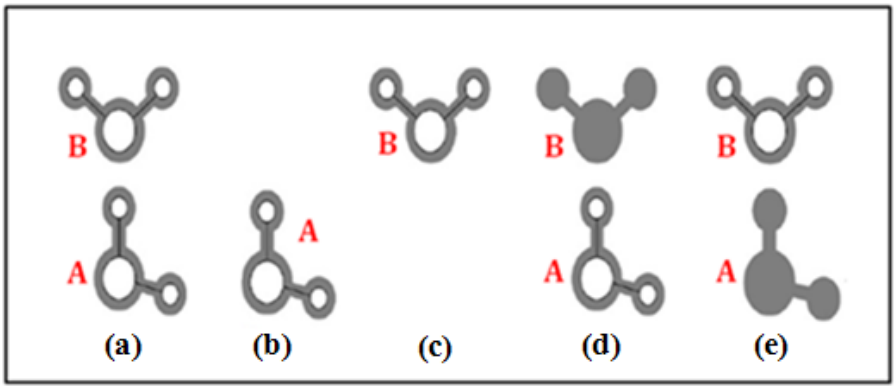

Figure 2.2. Illustrating the Counterpoise method to calculate the binding energy. (a) Represents the basis functions for total system where atoms are white colour and the basis functions of the atoms are gray. (b) and (c) show the basis function for the individual monomers whereas (d) and (e) represent the counterpoise correction, every single molecule is evaluated with the same basis function as the total system in (a) [60].

In Figure 2.2 a, b and c represent the two isolated molecules with their individual and corresponding basis functions while the shaded gray atoms in 2.2 d and e represent the ghost states (basis set functions which have no electrons or protons). The BSSE is obtained by recalculating using the mixed basis sets realised by introducing the ghost orbitals, and then subtracting the error from the uncorrected energy to calculate the binding energy E_{Bin} given by:

$$E_{Bin} = E_a - (E_d + E_e) \qquad (2.35)$$

where E_a, E_d and E_e are the total energy of (a), (d) and (e) systems in figure 2.2, respectively. This is an important concept that has been successfully implemented in many systems to give reliable and realistic results [60, 61, 62].

2.6.3. Structure Optimisation

In this thesis, the SIESTA code is used to obtain the ground state energy of different atomic configurations, and then obtain the relaxed structure of the systems. This means that SIESTA can provide us the energy as a function of the atomic coordinates (position of atoms). The structure optimisation (also known as geometry optimisation) contains three options; relaxing atomic coordinates, allowing periodic cell shapes and volumes to change. In case of full optimisation, the three options can be employed together, which leads to the minimum energy of the atoms in the system and the equilibrium lattice parameters of the systems. Performing the relaxation of the atomic positions allows atoms to move until the residual force between all atoms is smaller than the required convergence tolerance in eV/Å. In structural optimisation the force is the key quantity and this force could be calculated numerically by taking the approximate numerical derivatives of the total energy with respect to the positions. This method is applied in SIESTA using the Hellmann-Feynman theorem [63].

2.7. Green's Function Scattering Formalism

To calculate the transmission coefficient of a molecule connected to semi-infinite leads we use a Green function scattering formalism. This is a further step after calculating the electronic structure of an isolated molecule or molecular wire by using DFT which was explained in previous chapter.

The electronic properties of an open a system are influenced by both the properties of the isolated molecule and the contact between the molecule and electrodes. So transport calculations need to include both features to understand the scattering process of an electron between the two electrodes. In contrast to the wave function φ, which satisfies[64]:

$$(E-H)\phi=0 \quad \text{…….. (2.36)}$$

The Green function satisfies

$$(E-H)G=I \quad \text{……. (2.37)}$$

Formally this is solved by Dyson's equation which is

$$G=(E-H)^{-1} \quad \text{……. (2.38)}$$

To avoid the singularities in (2.38) which happen when an eigenvalue of *H* is equal to energy *E*. we add a small imaginary part to *E*:

$$G_{\pm}=\lim_{\eta\to 0}(E-H\pm i\eta)^{-1} \quad \text{……. (2.39)}$$

The sign of the positive infinitesimal η determines the type of solution which is either a retarded (-) or advanced (+) Green function. Generally, the methodology of computing electron transport is focused on computing a Green function for the infinite system, which includes the leads and the scattering region.

2.8. Landauer Formula

The conductance G is given by the Landauer formula:

$$\mathbf{G}=\frac{2e^2}{h}T(\mu) \quad \text{…….. (2.40)}$$

Where T(μ) is the transmission coefficient as a function of the chemical potential μ and the quantum conductance G_0 represented by $2e^2/h$. The quantity G_0 includes the factor of 2 in the formula to include spin degeneracy. Equation (2.40) describes the relation between the probability for an electron to transfer from one lead to the other and the experimentally measurable quantity G[65].

The transport model will be used in Figure 2.3 to discuss the Landauer formula in more detail. This model involves interconnected leads with a scatterer and two infinite electron reservoirs connected to the free terminations of the leads. There is a small chemical potential difference $\mu_L - \mu_R = \delta E > 0$ between opposite model sides that allows the movement of electrons from left to right with an energy condition where $\mu = \mu_L \approx \mu_R$.

For one open channel, the incident current is given by

$$\delta\hat{I} = ve\frac{\partial n}{\partial E}\delta E \quad \text{..... (2.41)}$$

The density of states per unit length $\partial n / \partial E$ is related to the group velocity v at energy μ by

$$\frac{\partial n}{\partial E} = \frac{1}{2\pi}\frac{\partial k}{\partial E} = \frac{1}{vh} \quad \text{..... (2.42)}$$

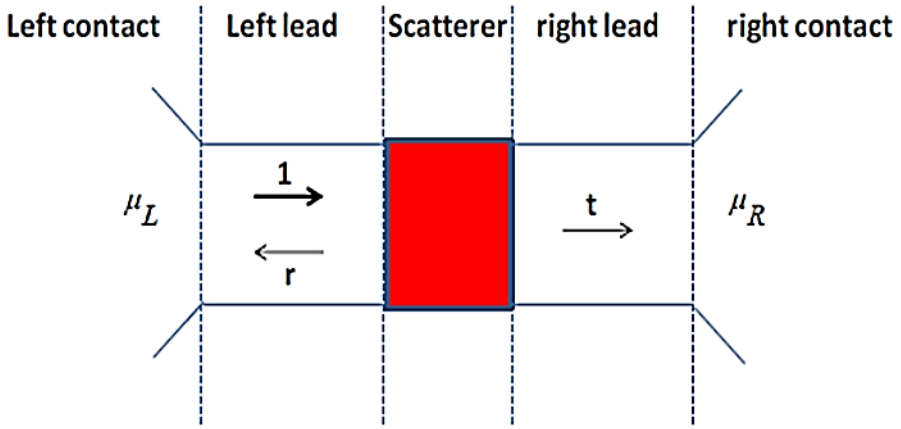

Figure 2.3. Theoretical One-dimensional Transport Model [66].

The current will then be $\delta I\hat{}= (2e/ h)\ \delta E = (e^2 /h)\ \delta V$, where δV is the voltage bias $(\mu_L-\mu_R)/e$ when electrons undergo reflection with probability R and are transmitted with probability T, the current will be

$$\delta\hat{I} = \frac{e^2}{h} T\delta V \quad \text{..... (2.43)}$$

More generally, when the leads contain more than one open channel,

$$T = \sum_{p,q} \left| t_{p,q} \right|^2 \quad \text{..... (2.44)}$$

The transmission amplitude is $t_{p,q}$ which describes the transport process from left channel q to right channel p. The conductance is then described by (2.40) when $G(\eta) = \delta I\hat{}/\ \delta V$. Finally, the description of all the transmission and reflection process for any system can be found in the scattering matrix S which contains the transmission and reflection amplitudes from left to right t and r, and the transmission and reflection amplitudes from right to left t' and r'.

$$S = \begin{pmatrix} r & t' \\ t & r' \end{pmatrix} \quad \text{..... (2.45)}$$

In what follows, *S* is computed for the retarded Green function *G(E)* of the system. *G(E)* is obtained by using Dyson's equation to couple the Green function of the leads to the Green function of the scattering region. Now, the charge and heat currents expressions in the linear bias and temperature regime describe the connection between current, heat, temperature and voltage which is represented by the generalized Landauer-Büttiker formulae included Fermi distribution function $f_j(E) = (1 + e^{(E-\mu_j)/k_b T_j})^{-1}$ where T_j is the temperature and k_b Boltzmann constant[66-67]. To clarify the generalized Landauer-Büttiker formulae, we consider model in Figure (2.3). All scattering effects will occur in the scattering region therefore I will consider the case where there is no scattering region and the reservoirs are connected to the leads in a way. So the right moving current of a single k-state which is coming from the left reservoir can be described by the number of electrons per unit length *n*, the Fermi distribution f_L and the group velocity *v*, therefore the transmission probability *T* is given by

$$I_k^+ = n\, e\, v(E(k))\, T(E(k))\, f_L(E(k)) \quad \ldots\ldots\ldots\ldots\ldots\ldots\ldots\ldots \quad (2.46)$$

The summation of all positive *k* states will give the total current from the right moving states then converting to the integral form by using $v = 1/\hbar\ (\partial E(k)/\partial k) = 2\gamma \sin(k)$ and $n = 1/L$.

$$I^+ = \sum_k e \frac{1}{L}\frac{1}{\hbar}\frac{\partial E(k)}{\partial k} T(E(k))\, f_L(E(k))$$
$$= \int_{-\infty}^{\infty} \frac{2e}{h} T(E)\, f_L(E)\, \mathrm{dE} \quad \ldots\ldots\ldots\ldots\ldots\ldots\ldots\ldots \quad (2.47)$$

The left moving states are

$$I^- = \int_{-\infty}^{\infty} \frac{2e}{h} T(E)\, f_R(E)\, \mathrm{dE} \quad \ldots\ldots\ldots\ldots\ldots\ldots\ldots\ldots\ldots\ldots \quad (2.48)$$

Therefore, the total current moving to the right is given by the famous Landauer-Büttiker formula shown in equation (2.49).

$$I = I^{+} - I^{-} = \frac{2e}{h}\int_{-\infty}^{\infty} T(E)(f_L(E) - f_R(\mathrm{E}))\,\mathrm{dE} \qquad \ldots\ldots\ldots\ldots\ldots\ldots\ldots\ldots (2.49)$$

The heat or energy current for the same system can be derived in same way by considering $\hat{Q} = Env$ and is given by

$$\hat{Q} = \hat{Q}^{+} - \hat{Q}^{-} = \frac{2}{h}\int_{-\infty}^{\infty} T(E)((E-\mu_L)f_L(E) - (E-\mu_R)f_R(E))\,dE \qquad \ldots (2.50)$$

$$f_L(E) = \left(1 + e^{(E-\mu-\Delta\mu/2)/(k_b(\mathrm{T}+\Delta\mathrm{T}/2))}\right)^{-1}$$

$$f_R(E) = \left(1 + e^{(E-\mu+\Delta\mu/2)/(k_b(\mathrm{T}-\Delta\mathrm{T}/2))}\right)^{-1}$$

$$\mu_{\mathrm{L}} = \mu + \Delta\mu/2, \qquad \mu_{\mathrm{R}} = \mu - \Delta\mu/2$$

$$\mathrm{T_L} = \mathrm{T} + \Delta\mathrm{T}/2, \qquad \mathrm{T_R} = \mathrm{T} - \Delta\mathrm{T}/2 \qquad \ldots\ldots\ldots\ldots\ldots\ldots (2.51)$$

2.9. GOLLUM Code

GOLLUM is a program that computes the charge, spin and electronic contribution to the thermal transport properties of multi-terminal junctions. In contrast to a non-equilibrium Green's function (NEGF) codes, GOLLUM is based on equilibrium transport theory, which means that it has a simpler structure, is faster, and consumes less memory. The program has been designed for user-friendliness and takes a considerable leap towards the realization of *ab initio* multi-scale simulations of conventional and more sophisticated transport functionalities.

The simpler interface of GOLLUM allows it to read model tight-binding Hamiltonians. Furthermore, GOLLUM has been designed to interface easily with any DFT code that uses a localized basis set. It currently reads information from all the latest public flavors of the code SIESTA [68]. An interface to the code FIREBALL [69] is under development. These include functional that handle the spin–orbit or the van der Waals interactions or include strong correlations in the spirit of the local density approximation (LDA) approach. Plans to generate interfaces to other codes are underway. Two- and three-dimensional (3D) topological materials display fascinating spin transport properties. GOLLUM can simulate junctions made of these materials using either parametrized tight-binding Hamiltonians [66,70] or DFT[71]. DFT does not handle correctly strong electronic correlation effects that are inherent in many nano-scale electrical junctions. As a consequence, a number of NEGF programs like SMEAGOL underestimate such effects. GOLLUM includes several tools to handle strong correlations. These include the above-mentioned interface to the versions of SIESTA containing the LDA+U functional. A second tool uses a phenomenological but effective approach called the scissors correction scheme. A third tool maps the DFT Hamiltonian into an Anderson-like Hamiltonian that is handled with an impurity solver in the spirit of dynamical mean field theory.

2.10. Electric and Thermoelectric Properties

Rotaxane molecules have attracted a wide range of interest due to their unique electric and thermoelectric characteristics, as they have potential applications in molecular electronics and thermoelectric devices. The electrical conductance of rotaxane molecular junctions can be affected by the chemical composition of the molecule, as well as the number, size and shape of the wheels and the axle [72].

The transport properties is then calculated using the Landauer formula:

$$G(E_F T) = G_{\circ} \int_{-\infty}^{\infty} dE\, T(E)[-\partial f(E,T,E_F)/\partial E] \quad \ldots\ldots\ldots\ldots\ldots\ldots (2.52),$$

where

$$f = \left[e^{(E-E_F)} /_{k_B} T + 1 \right]^{-1} \quad \ldots\ldots\ldots\ldots\ldots\ldots\ldots\ldots\ldots\ldots\ldots\ldots\ldots\ldots (2.53)$$

is the Fermi-Dirac probability distribution function, T is the temperature, E_F is the Fermi energy, $G_{\circ} = (2e^2)/h$ is the conductance quantum, e is electron charge and h is the Planck's constant. DFT can give inaccurate value for the Fermi energy that the calculated conductance are obtained for a range of Fermi energies [73]. The thermopower or Seebeck coefficient S is defined as the difference of electrochemical potential per unit temperature difference developing across an electrically isolated sample exposed to a temperature gradient. The Seebeck coefficients and power factors is also informative. Provided the transmission function, T(E), can be approximated by a straight line on the scale of K_{BT}, the Seebeck coefficient is given by:

$$S \approx -L|e|T \left(\frac{dln\, T(E)}{dE} \right)_{E=E_F} \ldots\ldots\ldots\ldots\ldots\ldots\ldots\ldots\ldots\ldots\ldots\ldots (2.54)$$

Where L is the Lorenz number $L = \left(\frac{k_B}{e}\right)^2 \frac{\pi^2}{3} = 2.44 \times 10^{-8}\, W$. In other words, S is proportional to the negative of the slope of ln T(E), evaluated at the Fermi energy.

The power factor is the ratio of the real power absorbed by the load to the apparent power flowing in the circuit. Real power is the average of the instantaneous product of voltage and current and represents the capacity of the electricity for performing work. From the Seebeck coefficient, the power factor was calculated as given in equation (2.55)

$P = GS^2\, T$ ……………………………… (2.55)

, where T is the temperature T = 300 K, G is the electrical conductance and S is the thermopower.

In conventional devices the maximum efficiency of either heat transfer or current generation is proportional to the dimensionless thermoelectric figure of merit. The common measure for thermoelectric efficiency is given by the figure of merit, which is given by [74]:

$ZT = \frac{GS^2}{k_{el}+k_{ph}}T$ …….. (2.56), where G is the electrical conductance, S is the thermopower, k_{el} is the electron thermal conductance, $k_{ph}$is the phonon thermal conductance. The figure of merit is determined from the thermoelectric transport coefficients in equations (2.54), (2.57),(2.58), and (2.60) in the linear response regime [75-76].

$G = \frac{2e^2}{h}k_0$ …….. (2.57)

$k_{el} = \frac{2}{hT}\left(K_2 - \frac{K_1^2}{K_0}\right)$ …….. (2.58)

In the expressions $e = |e|$ is the absolute value of the electron charge, h is the Planck constant, and $T = (T_L + T_R)/2$ is the average junction temperature. The coefficients in (2.57) and (2.58) are defined as:

$k_n = \int dE\, T_{el}(E)\left(-\frac{\partial f(E)}{\partial E}\right)(E-\mu)^n$ …….. (2.59)

Where $T_{ph}(E)$ is the electron transmission, and the chemical potential $\mu \approx E_F$ is approximately given by the Fermi energy E_F of the Au electrodes.

The corresponding thermal conductance due to the phonons is given in linear response by:

$k_{ph} = \frac{1}{h}\int_0^\infty dE\, ET_{ph}(E)\frac{\partial n(E,T)}{\partial T}$ …….. (2.60)

Where $T_{ph}(E)$ is the phonon transmission and $n(E,T) = \{\exp(E/k_BT) - 1\}^{-1}$ is the Bose function, characterizing the phonon reservoirs in the left and right electrodes.

Hence, an upper bound for ZT in the limit of vanishing phonon thermal transport $\kappa_{ph} \rightarrow 0$ is given by the purely electronic contribution [75] as

$$Z_{el}T = \frac{S^2 G}{k_{el}} T = \frac{S^2}{L} \quad \text{..... (2.61)}$$

Hence, the Lorenz number is $L = \kappa_{el}/GT$. With $Z_{el}T$, and depending on above the figure of merit is presented in a slightly different form as:

$$ZT = \frac{Z_{el}T}{1+{}^{k_{ph}}/_{k_{el}}} \quad \text{..... (2.62)}$$

3.1. Structural and Morphological Properties

A rotaxane is a mechanically interlocked molecular architecture consisting of a linear molecule (the axle) that is threaded through a macrocycle (the wheel). The wheel and axle components are typically held together by non-covalent interactions, such as hydrogen bonding or coordination bonds. The structural and morphological features of a rotaxane molecule can very depending on the specific design of the molecule [77]. However, in general , a rotaxane molecule can be described as having three main parts: the wheel, the axle, and the stoppers. The wheel is typically a cyclic molecule with a cavity that is large enough to accommodate the axle. The wheel can be made from a variety of cyclic compounds, such as crown ethers, cyciodextrins, or calixarenes. The size and shape of the wheel can be tailored to fit the specific properties of the axle. The axle is a linear molecule that is threaded through the cavity of the wheel. The structural and morphological features of a rotaxane molecule are designed to create mechanically interlocked architecture that can exhibit unique properties, such as molecular switching or molecular machines [78].

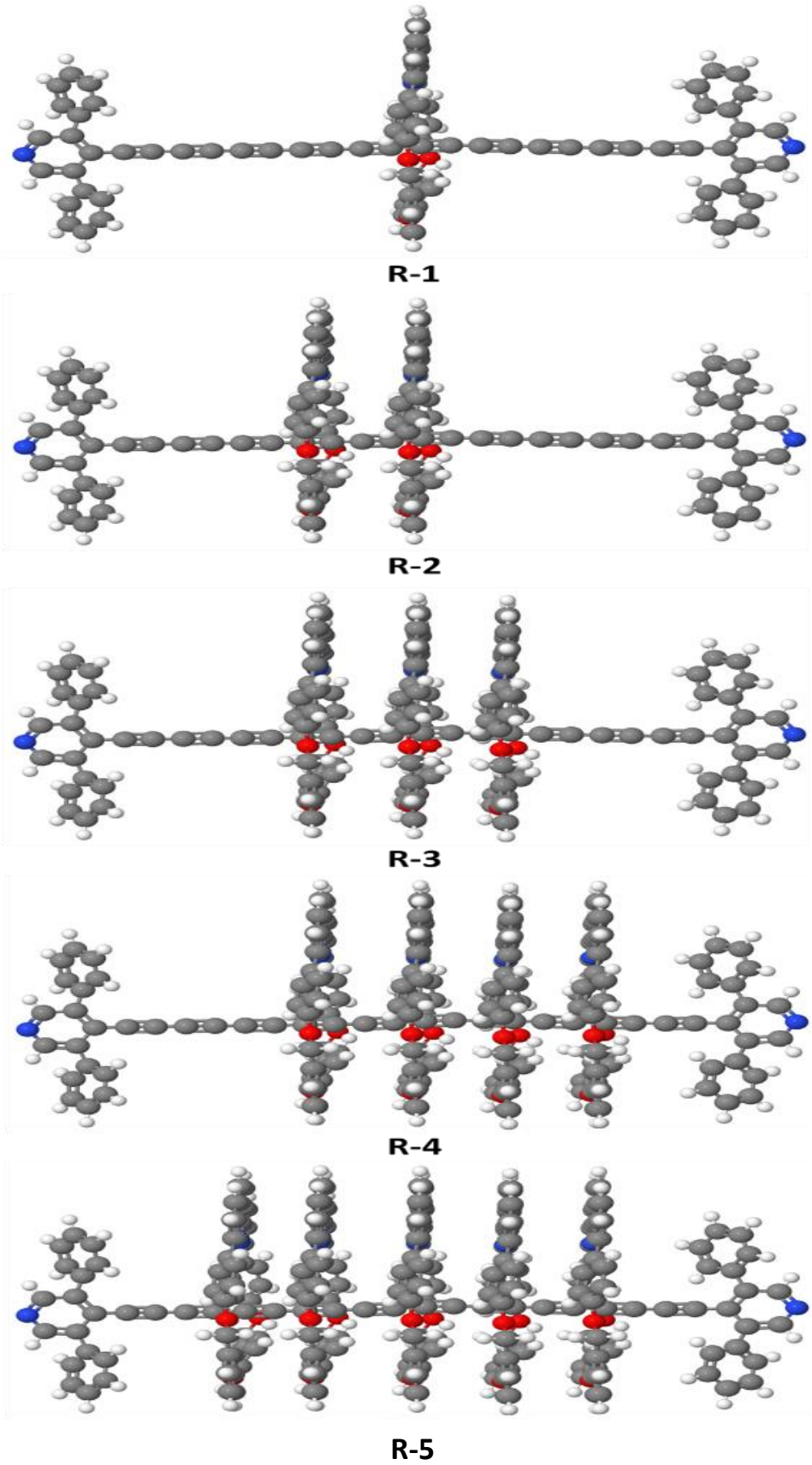

Figure 3.1. The optimized geometries at ground state of all molecules. The red balls are oxygen atoms, grey are carbon atoms, the white ones are hydrogen atoms, and the blue ones are nitrogen atoms.

The most basic rotaxane shape consists of a rod-like axle and a ring torus shaped wheel that is threaded on the axle as shown in the Figure 3.1. The wheel part is not covalently bonded to the axle part and is free to move along the axis .This work involves five different rotaxane molecules, which are identicale in their backbone (the axle) and differ in the number of rings (macrocycle wheels). The number of rings has been increased from one ring for molecule R-1 to five rings for molecule R-5. The backbone of the rotaxane molecules ends with an achor groups called stoppers. The stoppers are bulky groups attached to the ends of the axle that prevent rings from slipping out of the wheel cavity.

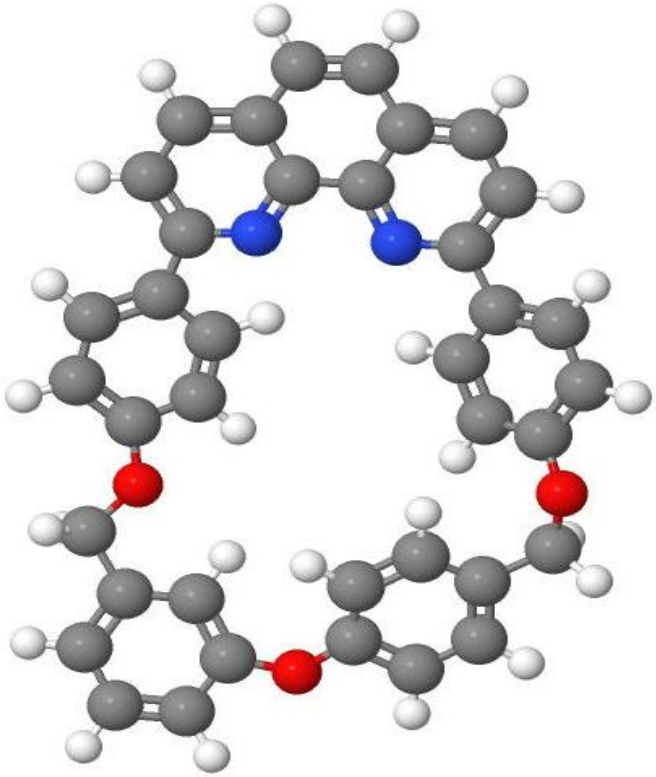

Figure 3.2. The optimized geometry at ground state of macrocycle wheel. The red balls are oxygen atoms, grey are carbon atoms, the white ones are hydrogen atoms, and the blue ones are nitrogen atoms.

The stoppers consistis of phenyl rings attached to pyridine ring, which is the bonding ring of the molecule. The axle is composed of nine carbon-carbon triple bonds and nine of carbon-carbon single bonds atoms, which

result in an important property called the π-conjegated structure [3]. The wheel is typically a cyclic molecule consiste of phenyl rings linked to pyridine rings at the upper part, while the lower part consiste of phenyl rings combined with three oxgen atoms as shown in Figure 3.2.

Table 3.1. The structural aspect of all molecules. L is the molecule length. C–H is the carbon-hydrogen single bond. C–C is the carbon-carbon single bonds. C=C is the carbon-carbon double bonds.C≡C is the carbon-carbon triple bonds. C–N is the carbon-nitrogen single bonds. C–O is the carbon-oxygen single bonds.

Molecule	No. of rings	No. of atoms	L (nm)	C–H (nm)	C–C (nm)	C=C (nm)	C≡C (nm)	C–N (nm)	C–O (nm)
R-1	1	149	3.367	0.108	0.141	0.139	0.118	0.134	0.146
R-2	2	218	3.163	0.108	0.141	0.139	0.118	0.134	0.146
R-3	3	286	3.17	0.108	0.141	0.139	0.118	0.134	0.146
R-4	4	354	3.188	0.108	0.141	0.139	0.118	0.134	0.146
R-5	5	422	3.198	0.108	0.141	0.139	0.118	0.134	0.146

It is obvious that the number of atoms increase with increasing the number of macrocycle wheels, since it raise from 149 atoms for R-1 to 422 atoms for R-5. In addition, the molecule length has been fluctuated slightly form molecule to another one, and this could be ascribed to the effect of wheels.

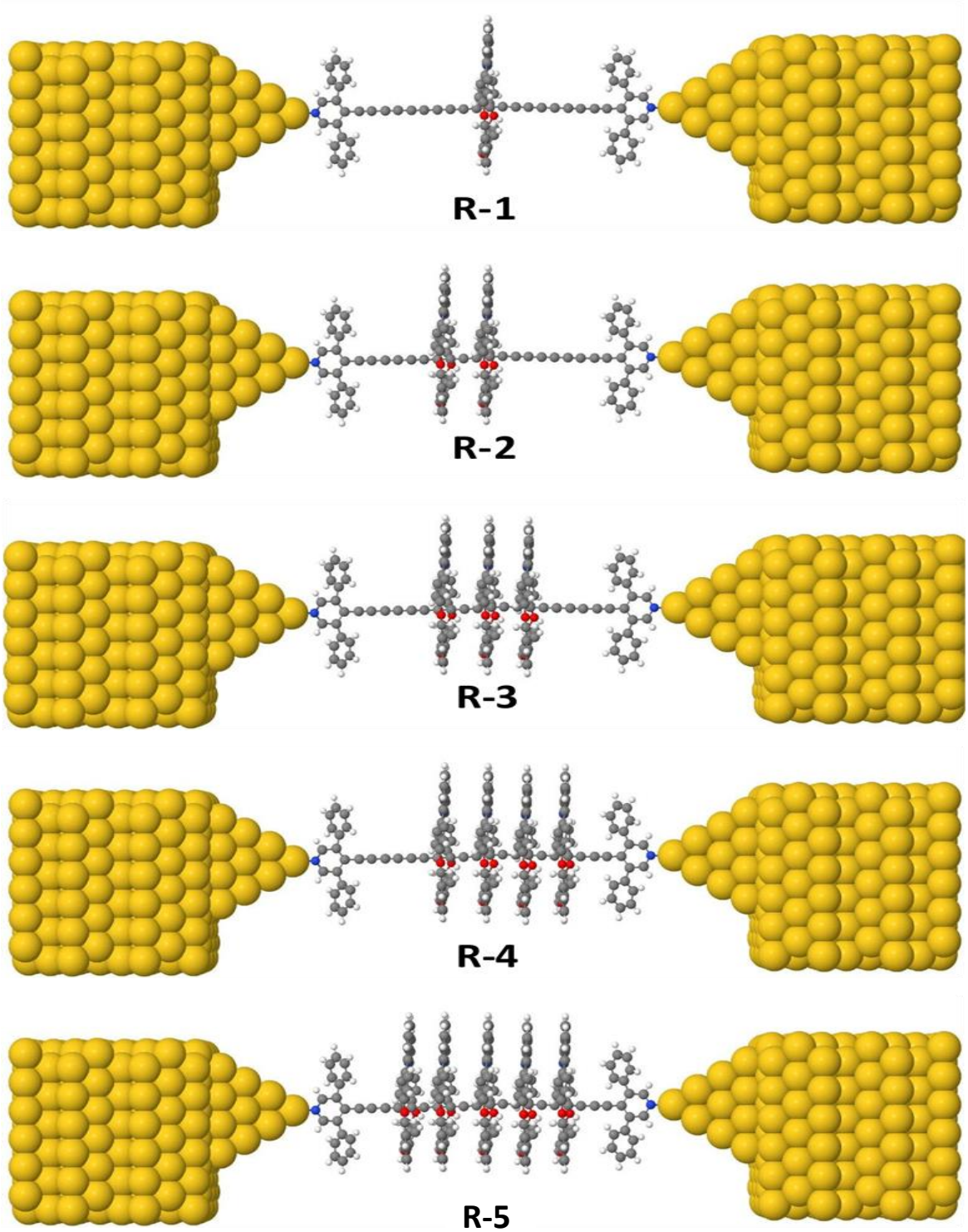

Figure 3.3. The optimized geometries at ground state of all molecular junctions.

To obtain the optimized geometries of all systems under investigation in this work, and to compute the electrical conductance and thermopower, the density functional theory (DFT) methods (the SIESTA code), and a non-

equilibrium Green's function formalism [79,80], were utilized. For the transmission and Seebeck coefficients calculations, the molecular junction was created by attaching the relaxed molecule to 35-atom pyramidal gold electrodes as shown in Figure 3.3, with 8 base layers, each layer consisting of 6×6 atoms and a layer spacing of 0.235. For more details see [81-82]. From these model junctions the conductance and thermopower, were calculated using the GOLLUM code [81]. All molecules in this study were initially geometrically relaxed in isolation to yield the geometries presented in Figure 3.1. To investigate ideal junction geometries, a small four-atom gold pyramid was attached to the N atoms of the molecules, with Au–N–C angle being 120° and Au–N bond length being 0.23 nm, as shown in Figure 3.3. Geometrically optimization were carried out using the DFT code SIESTA, with a generalized gradient approximation [83,84] (PBE functional), double ζ polarized basis set, 0.01 eV/A force tolerance, a real-space grid with a plane wave cut-off energy of 250 Ry, zero bias voltage and 1 k points.

It is clear that the molecule length have fluctuated slightly for all molecules in molecular junction. This is could be interpreted in terms of an excitations state due to the electrons transport from left electrode through the molecule to the right electrode.

Table 3.2. The structural aspect of all molecular junctions. L is the molecule length. d is the molecular length (Au … Au). Z is the theoretical electrode separation (Z = d – 0.25), where 0.25 is the quantum conductance. X is the gold-nitrogen bond (Au–N).

Molecule	L (nm)	d (nm)	Z (nm)	X (nm)
R-1	3.367	3.827	3.577	0.23
R-2	3.163	3.618	3.368	0.23
R-3	3.17	3.624	3.374	0.23
R-4	3.188	3.643	3.393	0.23
R-5	3.198	3.652	3.402	0.23

3.2. Electronic Properties

The electronic characteristics of rotaxane molecules depend on the specific design and composition of the molecule. However, the electronic properties of rotaxanes can be influenced by the presence of the macrocycle and the axle, as well as the nature of their interactions [85].

The macrocycle in a rotaxane can act as an electron donor or acceptor, depending on its functional groups and the nature of its interactions with the axle [86]. In addition, the electronic properties of the axle can also influence the electronic characteristics of the rotaxane. For example, the axle can have different types of functional groups that can donate or accept electrons, or it can have a specific electronic structure that can defect the interactions with the macrocycle. The nature of the interactions between the macrocycle and the axle in a rotaxane can also affect the electronic characteristics of the molecule. For example, the presence of hydrogen bonding or coordination bonds between the macrocycle and the axle can lead to changes in the electronic structure and properties of the molecule.

3.2.1. Transmission Coefficient T(E)

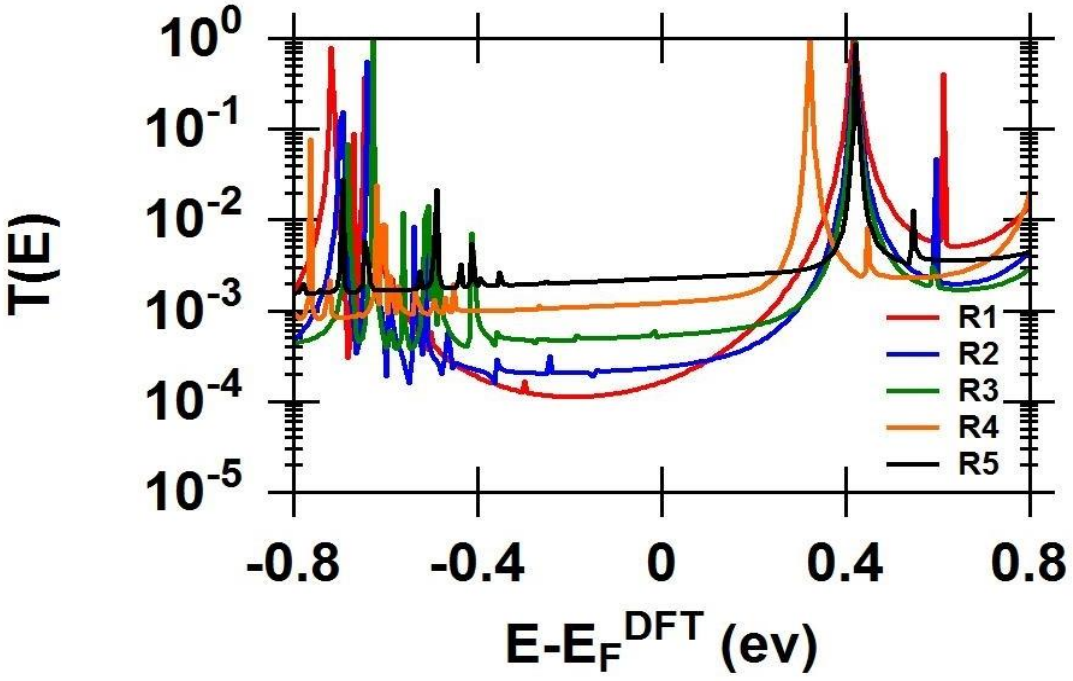

Figure 3.4. Represents the transmission coefficient T(E) as a function of electrons energy of all molecular junctions.

The transmission coefficient T(E) is a property of the whole system comprising the leads, the molecule and the contact between the leads and the molecule. Nevertheless, if the contact to the electrodes is weak, then a graph of T(E) versus E will reflect the energy-level structure of the isolated molecule. In general, the transmission coefficient T(E) describing the propagation of electrons of energy E from the left to the right electrodes. In this thesis, the transmission coefficient have been calculated by first obtaining the corresponding Hamiltonian and overlap matrices using SIESTA and then using the GOLLUM code. Figure 3.4 shows that R-5 introduces a high value of transmission coefficient (2.23×10^{-3}), while the lowest value of the transmission (1.61×10^{-4}) is presented by molecule R-1. The order of the transmission is $T(E)_{R-5} > T(E)_{R-4} > T(E)_{R-3} > T(E)_{R-2} >$

$T(E)_{R-1}$. These outcomes could be explained in terms of the increasing of the donor atoms (oxgen atoms) at the wheels. That means is the raising of oxgen atoms from 3 atoms for R-1 to 15 atoms for R-5, leads to a sginficant raising in the transferred electrons Γ as shown in Figure 3.5, which leads to increase the value of transmission coefficient. Furthermore, the rings can act as additional pathways for electrons to pass through the molecule, providing more channels for conduction. What is more, the rings can also affect the geometry and orientation of the molecule, which can influence the overlap between the molecular orbitals involved in electron transport. As a result, the electronic coupling between the rings and the rest of the molecule can increase, leading to a higher transmission coefficient.

On the other hand, it can be seen that the transport mechanism for molecules are a LUMO-dominated transport, and this ascribed to type of anchor groups, which is the pyridine anchor group. This result is consistent with previous studies [87-88].

3.2.2. The Charges Transfer (Γ)

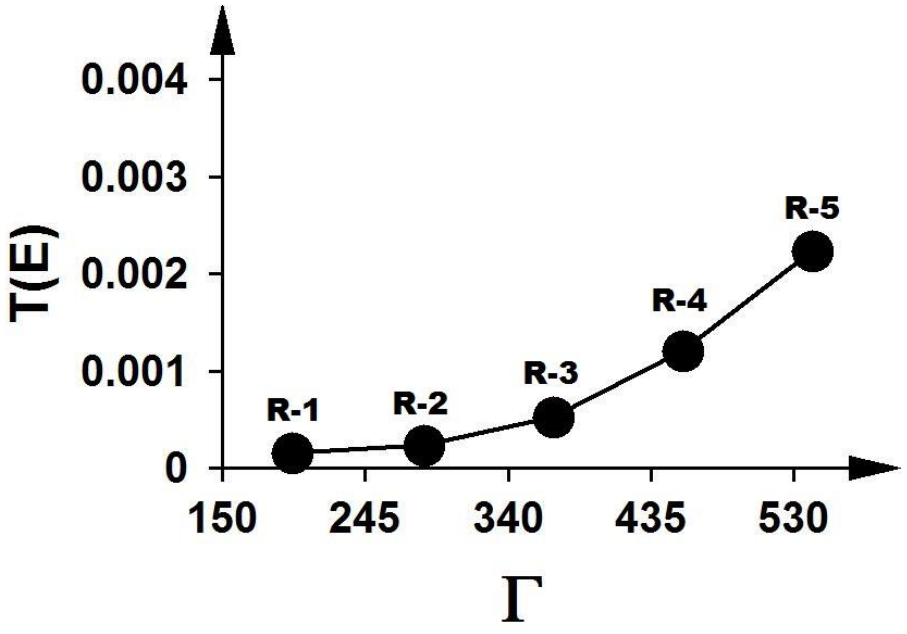

Figure 3.5. Represents the transmission coefficient T(E) as a function of the number of electrons transferred from molecule to electrodes of all molecular junctions.

Figure 3.5. shows that the number of electrons transferred from the molecules to the electrods ($\Gamma = \Gamma_M - \Gamma_{ME}$), sine Γ equals the number of electrons on the molecule in gas phase (Γ_M) minus the number of electrons on molecule in a junction (Γ_{ME}). It is true that the transmission coefficient increased with increasing of the Γ. This results could be attributed to the increasing of wheels, which leads to increasing the donor atoms (oxgen atoms). From another window, this result could explained in terms of the quantum size effect, which is one of the phenomena of nanomaterials. The rotaxane molecule consists of atoms that are linked to each other by bonds. These bonds are energy barriers for electrons to cross between atoms, and therefore the increasing of wheels leads to increasing the number of atoms, and that results in increasing the barriers, which inhibited recombination process between electrons and holes and increase the number of free electrons, and this consequences to a high or low transmission coefficient.

Table 3.3. Shows the energy levels HOMOs (the highest occupied molecular orbital), and LUMOs (the lowest unoccupied molecular orbital). T(E) is the transmission coefficient. Γ is the number of electrons transferred from molecules to electrodes. H-L gap is the energy gap between the HOMO and LUMO.

Molecule	T(E)	Γ	HOMO (ev)	LUMO (ev)	H–L gap (ev)
R-1	1.6×10^{-4}	196.6	-0.72	0.42	-1.14
R-2	2.4×10^{-4}	283.8	-0.69	0.42	-1.11
R-3	5.2×10^{-4}	369.9	-0.67	0.42	-1.09
R-4	1.2×10^{-3}	455.9	-0.76	0.31	-1.07
R-5	2.3×10^{-3}	542.0	-0.63	0.42	-1.05

Table 3.3 shows that the number of transferred electrons is 196.6 for molecule R-1, which is the lowest value. Whereas, the highest value is 542

electron for molecule R-5. In contrary, the table shows that the highest H-L gap is -1.14 eV for molecule R-1, while the lowest once is -1.05 eV for molecule R-5. These results predicates an important relationship between Γ, T(E), and H-L gap, since the increasing of Γ results in a high T(E), and low H-L gap, and vice-versa. These results as mentioned previously is ascribed to the quantum size effect phenomenon.

3.2.3. Electrical Decay Constant (β)

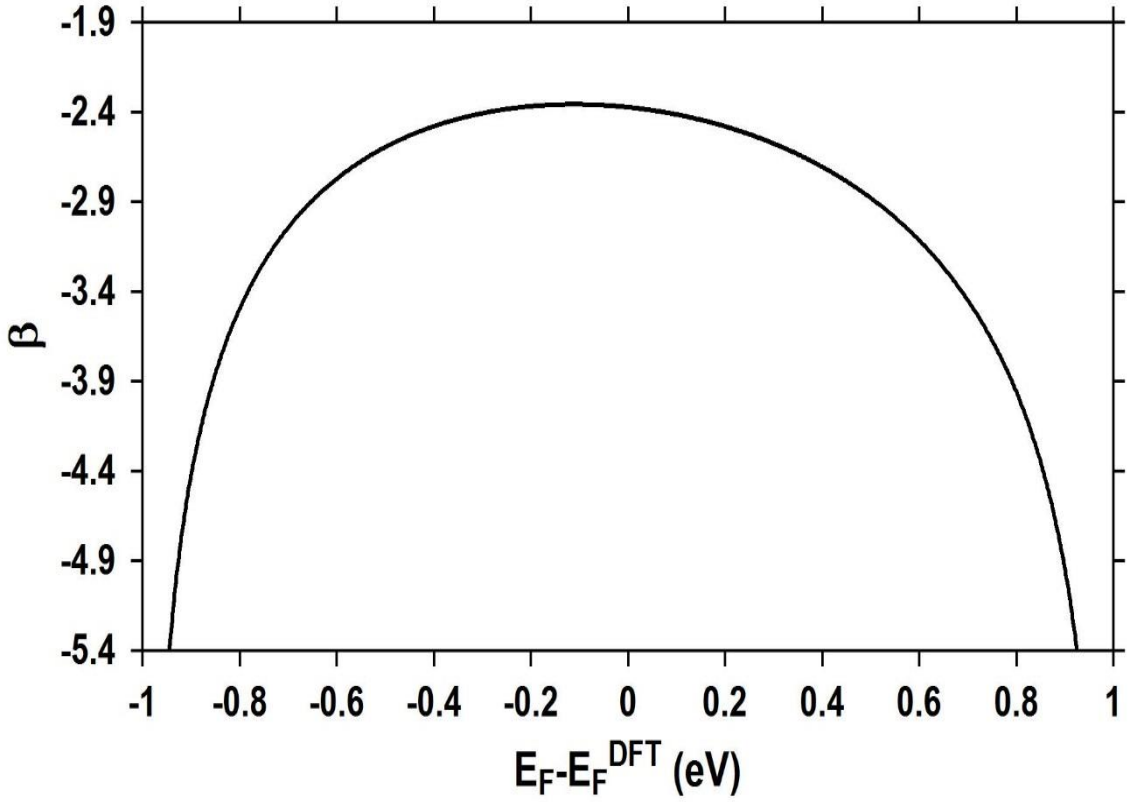

Figure 3.6. Represents the electrical decay constant (β) as a function of Fermi energy of all molecular junctions.

The decay constant in a rotaxane molecule is a measure of how quickly the electrical or electronic properties of the molecule decay as a function of distance [89]. The decay constant is related to the attenuation length, which is the distance over which the electrical or electronic signal carried by

electrons decays as it passes through the molecule. The decay constant can be calculated theoretically or measured experimentally, depending on the specific system and the properties of interest. We notice in Figure(3.6.) that at the beginning of the transfer of electrons and when the Fermi level is close to the Fermi level of the gold electrode, the values increase until the decay reaches its highest possible level at the middle of the homo-lumo gap. Then the values decrease until they reach the homo and lumo peaks, and this interpretation is completely consistent with Figure (3.4.),Since the lowest T(E) is at the middle of the homo-lumo gap in the position where the decay constant value is the lowest possible, we conclude that the calculations of the decay constant are supported by calculations of transmission Coefficient T(E).

For a simple single-channel, rectangular tunnel barrier model, conductance T(E) through the barrier (the molecule) decreases exponentially with the length of the barrier (L) as given equation (3.1)

$$T\ (E) = \ e^{-\beta L} \ \ldots\ldots\ldots\ldots\ldots\ldots\ldots\ldots\ (3.1)$$

Where β is the decay constant, L is the molecule length. This relationship has formed the basis of many explanations of transmission coefficient within families of similarly structured molecules, with the decay parameter, β, often serving as a proxy measure for the efficacy of wirelike behavior.

In the context of rotaxane molecules, the decay constant depends on various factors, such as the length and composition of the molecular wire, the nature of the linker groups between the rings and the axle, and the presence of functional groups on the rings or the axle. The decay constant can provide important information about the fundamental physics of electron transport in molecular wires, as well as the potential applications of rotaxanes in areas such as molecular electronics and sensing.

3.2.4. Binding Energy (B.E.)

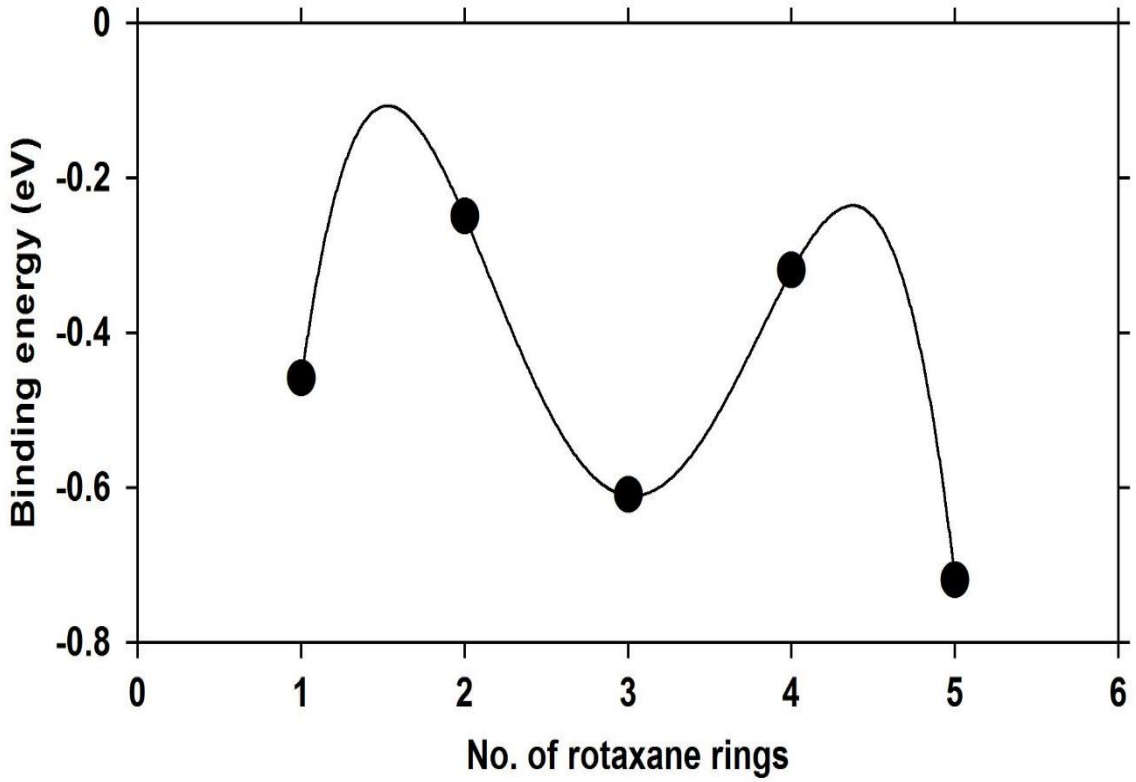

Figure 3.7. Represents the binding energy (B.E.) between molecule and gold electrodes of all molecular junctions.

The binding energy (B.E.) is the lowest energy required to make the system stable at an "equilibrium interaction distance". The binding energies between anchor groups and gold electrodes for the optimized configurations have been calculated. It is well known that SIESTA employs a localized basis set and therefore these calculations are subject to errors. Consequently, the counterpoise method has been used to obtain accurate energies [90]. This involves calculating the total DFT energies for the system ((Molecule plus gold (E_{MG})). The molecule alone (E_M), but with the same conformation adopted in the presence of gold electrode and in the absence of the molecule (E_G). For these energy calculations, the same basis functions as those generated for the system have been utilized. With these data the binding energies Eb have been calculated according to the expression as shown in equation 3.2 [91].

$BE = (E_{MG} - E_M - E_G)$ …… (3.2)

In this study the binding energy refers to the strength of the intermolecular interactions between the wheels and the axle that hold the molecule together, and therefore equation 3.2 could be writen as:

$BE = (E_{AB} - E_A - E_B)$ …… (3.3)

Where E_{AB} is the total energy of the system involves wheels and the axle. E_A is the total energy of the system but with the same conformation adopted in the presence of axele, while E_B is the total energy of the system in the absence of the axele.

Figure 3.7 predicates that the value of binding energy of rotaxane molecules has been fluctuated from -0.46 eV for R-1, then it decreased to -0.25 eV for R-2. Sharply, it raised to -0.61 eV for R-3, and again it lowered to -0.32 eV for R-4. Dramatically, the binding energy increased to the highest value -0.72 eV for R-5. These results reflect an important result to design the rotaxane molecule for drug delivery applications, since the rotaxane molecule with odd numbers of wheels leads to the highest values of binding energies, and this feature is main character for this kind of applications.

3.3. Electric and Thermoelectric Characteristics

3.3.1. Electrical Conductance (G/G_0)

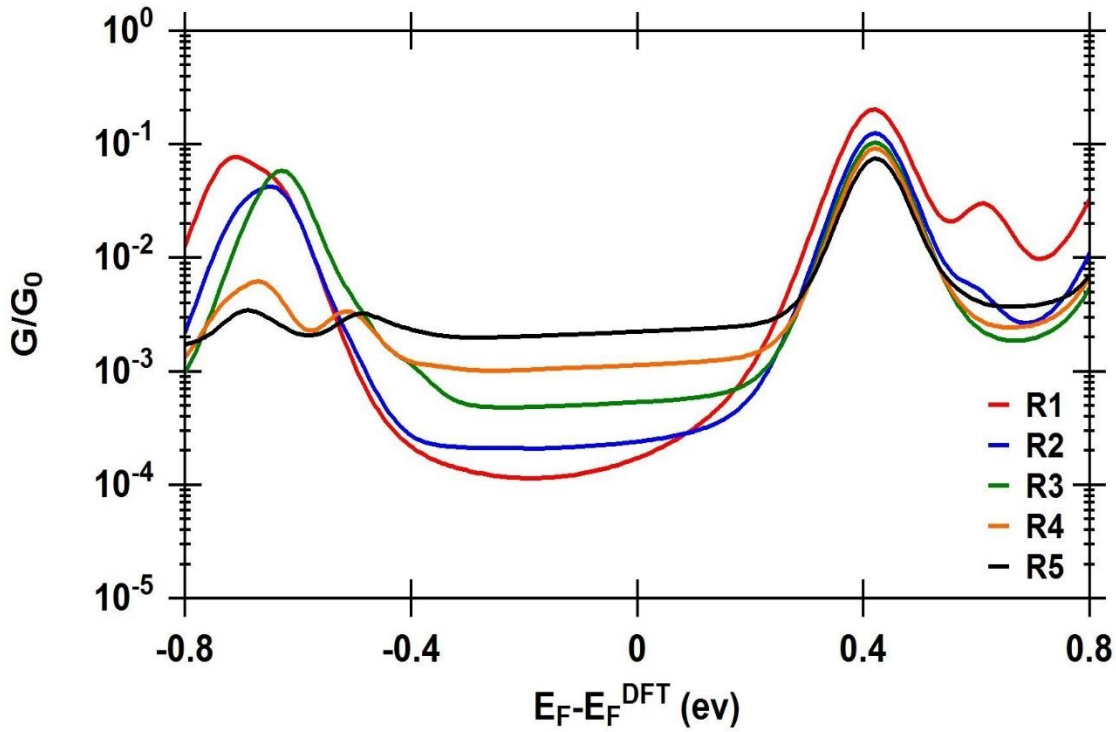

Figure 3.8. Represents the electrical conductance (G/G_0) as a function of Fermi energy of all molecular junctions.

Figure 3.8 shows that the highest electrical conductance is presented by R-5, while the lowest once is introduced via R-1, as well as the conductance raise with increasing the number of wheels in rotaxane molecule. These results could be interpreted in terms of the band theory of solids, since the increasing of number of wheels results in increasing in the electronic density of states at the Fermi level, which increases the intensity of LUMO resonance peaks as shown in Figure 3.8., which increases the conductance. In addition, the existence of multi-wheels in rotaxane molecule drives to an important impact of the electric field on the charges distribution and the energy levels of the molecular orbitals, leading to an increase in conductance.

Table 3.4. Shows the electrical conductance (G/G_0). H_{PI} is the HOMO resonance peak intensity. L_{PI} is the LUMO peak resonance intensity. V_{th} is the threshold voltage.

Molecule	(G/G_0)	H_{PI} (eV)	L_{PI} (eV)	V_{th} (eV)
R-1	1.5×10^{-4}	7.6×10^{-2}	2×10^{-1}	0.47
R-2	2.3×10^{-4}	5.9×10^{-2}	1.3×10^{-1}	0.45
R-3	5.1×10^{-4}	4.3×10^{-2}	1×10^{-1}	0.44
R-4	1.1×10^{-3}	6.1×10^{-3}	9.2×10^{-2}	0.43
R-5	2.2×10^{-3}	3.4×10^{-3}	7.5×10^{-2}	0.42

Table 3.4 and Figure 3.8 illustrate an important result, which is the electrons transport mechanism, since the theoretical Fermi energy (0.0 eV) is located at the midle of the HOMO-LUMO gap close to the LUMO peak resonance. In addition, the intensity of LUMO peaks is higher than that of the HOMO peaks, the transport mechanism is a HOMO-dominated transport.

3.3.2. Current-Voltage Characteristics

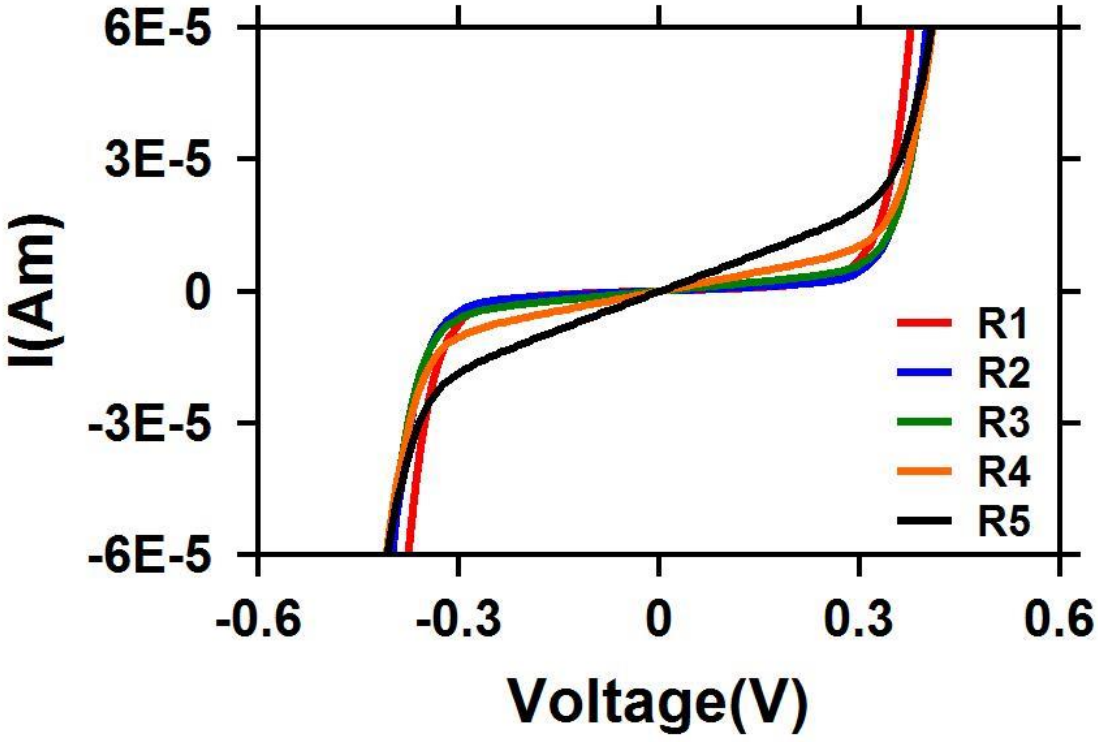

Figure 3.9. Represents the current-voltage (I-V) characteristics of all molecular junctions.

The current-voltage (I-V) characteristics of a rotaxane molecule describe the relationship between the current flowing through the molecule and the voltage applied across it. The I-V characteristics of a rotaxane molecule can exhibit various behaviors, ranging from ohmic to nonlinear behavior. In general, the I-V characteristics can be described by Ohm's law at low voltages, where the current is proportional to the voltage, and the electrical conductance of the molecule is constant. Analyzing the I–V curves in Figure 3.8 reflects many outcomes. The first one is the value of threshold voltage (V_{th})ranging from 0.47 eV for R-1 to 0.42 eV for R-5. This result means that the increasing of wheels in rotaxane molecules decrease the value of V_{th}. This is an important feature for electronic applications. The

second point is exhibited in the framework of the tunneling transport model, it could be identified those contacts are indeed formed by a single molecule. Under these conditions also symmetric coupling situations can be achieved that can be explained by physisorption of the end-groups to the electrodes. Rather high conducatnce in the range of 1.1×10^{-3} to 2.2×10^{-3} can be adjusted. Further, it has been demonstrated that the change of conductance is mainly achieved by tuning the coupling of the molecular orbital to the metal electrode while the dominant transport level E_0 remains mainly constant. The third point is the molecules favoured physisorption, since both the coupling and the energy of the frontier orbital can be tuned. These findings are important for the further improvement of photochromic molecules in future molecular electronic devices.

Furthermore, these results found rather broad distributions of conductance values in states. The analysis, based on the assumption that the current is carried by a single dominating molecular orbital, reveals distinct differences between states. Finally, these results predicated the appearance of light emitting diode-like behavior for the particular species pyridine (PY) that features end-groups, which preferentially couple to the metal electrode by physisorption.

3.3.3. Thermopower (S)

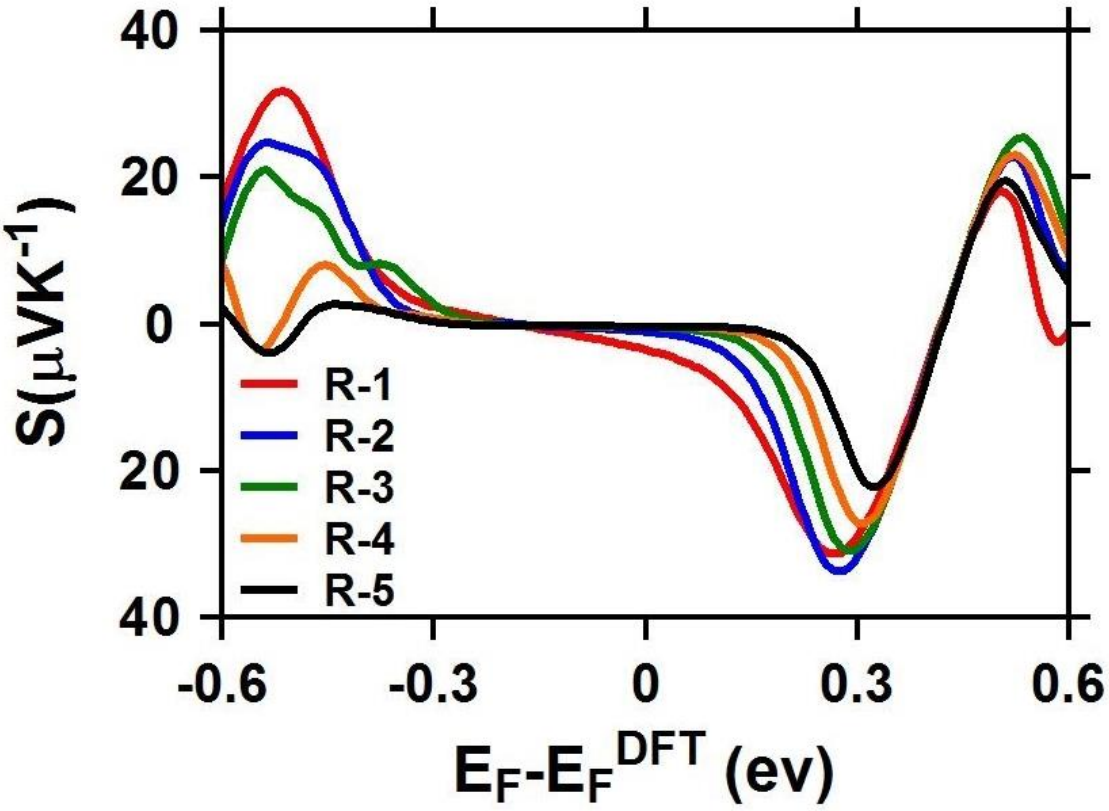

Figure 3.10. Represents the thermopower (S) as a function of Fermi energy of all molecular junctions.

The thermopower, also known as Seebeck coefficient, of a rotaxane molecule describes the magnitude and sign of the voltage generated across the molecule in response to a temperature gradient. The thermopower is a measure of the ability of the molecule to convert a temperature difference into an electrical signal, and is an important parameter for the development of thermoelectric materials and devices [92].

Thermopower is one of the most important properties for the thermoelectric applications. Figure 3.9 shows one of the most remarkable results of this work, which is the sign of the thermopower is negative, and that consistents with previous results that the transport mechanism is

LUMO-dominated transport. These results also demonstrated that there is a strong relation between the thermopower and electrical conductance, since the high thermopower -29 μVK^{-1} for molecule R-1 yields the lowest conductance as shown in Figure 3.8 and Table 3.4, whereas the low thermopower -19 μVK^{-1} for molecule R-5 gives the highest conductance. On the other hand, it could be observed that the thermopower value is very sensitivie to the position of the Fermi energy. This could be attributed to the delocalization of the electrons, leading to a higher degree of electronic mobility and a lower resistance to the flow of charge carriers, and that consequently leads to increase or lower the thermopower values.

3.3.4. Electronic Figure of Merit (ZT_e)

Figure of merit (ZT_e) is a metric used to evaluate the performance of a material for a specific application. In the case of a rotaxane molecule, the ZT_e would depend on the application of interest. For example, if the rotaxane molecule is being considered for use in a thermoelectric device, the ZT_e might be defined as the ratio of the electrical conductivity to the thermal conductivity multiplied by the Seebeck coefficient.

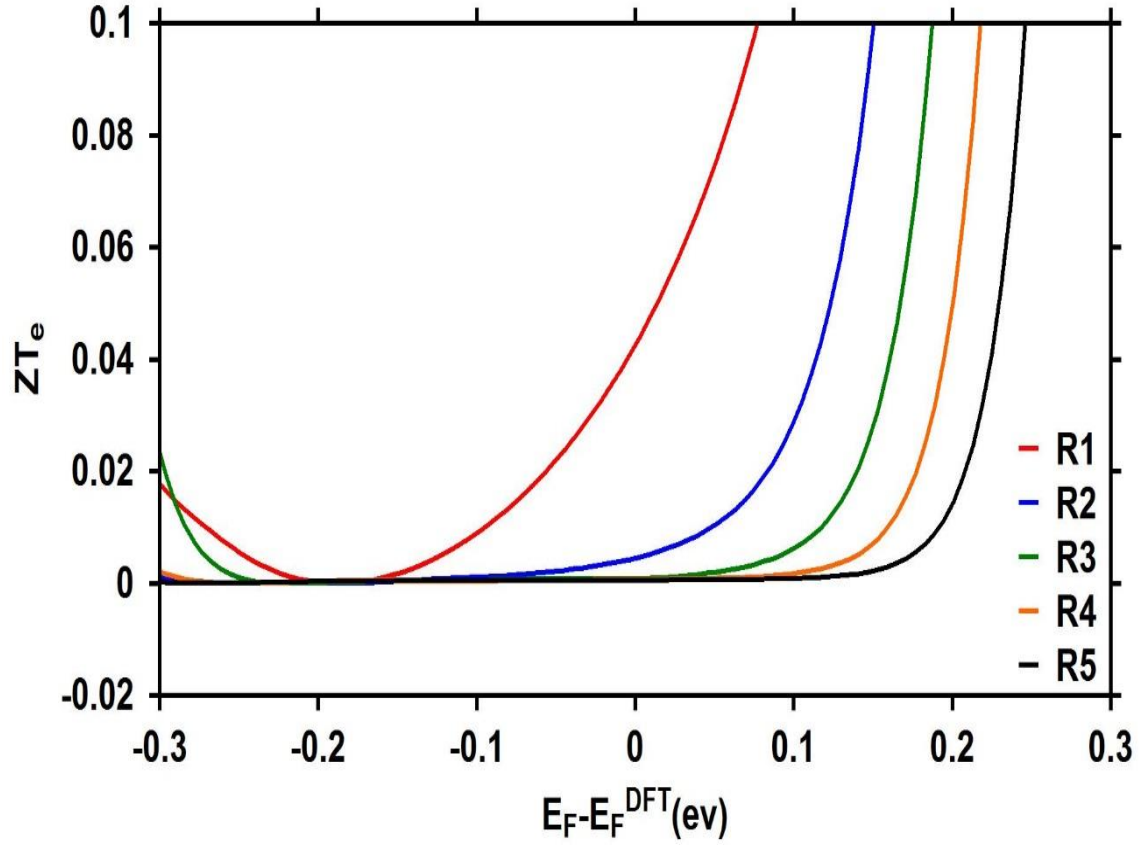

Figure 3.11. Represents the electronic figure of merit (ZT_e) as a function of Fermi energy of all molecular junctions.

In terms of low electrical conductance yields high thermopower, the results presented in table Figure 3.10 and Table and Table 3.5 show that the lowest conductance is introduced by R-1, which leads to a significant raising of electronic figure of merit value 0.04, and the highest value of Seebeck coefficient, while the highest conductance of molecule R-5 results in the lowest value 0.003 of ZT_e. In general, the values of the electronic figure of merit are low, and it is clear there is a stronge connection between electrical conductance, thermopower and figure of merit which definitely needs more investigations. Howevere, these results predicates that the changing of number of rotaxane wheels could be a promise strategy to influence, control and may be enhance the thermoelectric properties of this kind of molecular junctions.

Table 3.5. Shows thermopower (S), electronic figure of merit (ZT_e), and power factor (P).

Molecule	S μVK^{-1}	ZT_e	P $V^2/KSW \times 10^{-15}$
R-1	-29	0.05	1.2
R-2	-24	0.01	1.3
R-3	-22	0.009	2.4
R-4	-20	0.007	4.4
R-5	-19	0.006	7.9

3.3.5. Power Factor (P)

Figure 3.12. Represents the power factor (ZT_e) versus the number of wheels of all molecular junctions.

The power factor of any system is defined as the ratio of the real power absorbed by the load to the apparent power flowing in the circuit [93]. From the single-molecule conductance values, G, and the Seebeck coefficients, S, the power factor, P, which represents the capacity of a material to extract energy from the thermal difference, can also be determined as:

$P = GS^2 T$……. (3.4)

Thus, while the Seebeck coefficient of molecule R-1 is substantially higher than that of molecule R-5, the lower conductance of R-1 compound results in a lower overall power factor. These results bring to us an important results that the relation between electrical conductance and thermopower in terms of the competition, the impact of conductance is more dominant than that of thermopower in the case of rotaxane molecular junctions.

4.1. Conclusions

1- In conclusion, the results show that the structural and morphological characteristics such as the size, shape and number of axle and macrocycle wheels in rotaxane molecule are important parameters that determine not only the structural aspects but also the electronic and thermoelectric properties.

2- The transmission coefficient values were high and this an evidence of the constructive interference, which has been controlled and enhanced via changing the number of wheels in rotaxane molecules. In addition, the increasing of wheels number impacted the HOMO-LUMO gap, and this contributed in raising or lowering the transmission coefficient values.

3- It could be concluded that the mechanism of charges transport is LUMO-dominated electrons transport that is consistent with type of anchor groups, which are the pyridine anchor groups.

4- The smaller value of threshold voltage of all molecular junctions is a useful property for different applications.

5- All concluded results in points 2, 3, 4, 5 and 6 introduce a strong suggestion that the molecular junctions based on rotaxane molecules are promising candidates for electronic applications.

6- An important conclusion could be drawn from this work that the rotaxane molecules with odd numbers of wheels leads to the highest values of binding energies. This result proposes robustly that the rotaxane molecules are vigorous candidates for drug delivery applications.

7- A remarkable conclusion introduce itself from this work, which is the strong relationship between electrical conductance, thermopower and

figure of merit which definitely needs more investigations. In general, the highest conductance yields to low thermopower and figure of merit.

8- The results of power factor bring to us an important conclusion, which is that the relation between electrical conductance and thermopower in terms of the competition, the impact of conductance is more dominant than that of thermopower in the case of rotaxane molecular junctions.

9- Although the values of the figure of merit are very low, the conclusions presented in 8 and 9 points and the fact that the sign of thermopower is negative encourage more investigations of this kind of molecules for thermoelectric applications.

4.2. Future Works

1- Study of optical characteristics of the molecular nanostructures based on Rotaxanes.

2- Study of quantum properties of rotaxane-based molecular structures with different molecular lengths.